macQsimal	Title **Quantum-enhanced OPM methods report**	Deliverable Number **D4.2**
Project Number **820393**		Version **Version 1.0**

H2020-FETFLAG-2018-2021

macQsimal

Miniature **A**tomic vapor-**C**ell **Q**uantum devices for **S**ens**I**ng and **M**etrology **A**pp**L**ications

Deliverable D4.2

Quantum-enhanced OPM methods report

WP4 – Miniature optically-pumped magnetometers

Authors: Morgan Mitchell (ICFO), Charikleia Troullinou (ICFO), Vito Giovanni Lucivero (ICFO)

Lead participant: ICFO

Delivery date: 30.06.2020

Deliverable type: Report

Dissemination level: Public

This work has received funding from the European Union's Horizon 2020 research and innovation programme under grant agreement No. 820393.

Revision History

Author Name, Partner short name	Description	Date
Morgan Mitchell (ICFO)	Start of document	26.03.2020
Charikleia Troullinou (ICFO)	Squeezed-light Bell-Bloom magnetometer	30.05.2020
Vito Giovanni Lucivero (ICFO)	Sub-mm active volume OPM	11.06.2020
Morgan Mitchell (ICFO)	Harmonization of different sections	12.06.2020
Jacob Reichel (LKB, CNRS)	Internal review	28.06.2020
Morgan Mitchell (ICFO)	Final version (v1)	30.06.2020

Abbreviations

AMOR	Amplitude-Modulated nonlinear Optical Rotation
AOC	Alignment-to-Orientation Conversion
ASN	Atomic Shot Noise
BAE	Back-Action Evading
BEC	Bose-Einstein Condensate
CNRS	Centre National de la Recherche Scientifique CNRS *(participating in macQsimal with the Laboratoire Kastler Brossel, LKB, macQsimal Beneficiary No. 6)*
CSS	Coherent Spin State
DFB	Distributed Feedback
FID	Free-Induction Decays
FWM	Four-Wave Mixing
GW	Gravitational Wave
HF	HyperFine
HWP	Half-Wave Plate
ICFO	Fundacio Institut de Ciencies Fotoniques *(The Institute of Photonic Sciences, macQsimal Beneficiary No. 4)*
LHS	Left-Hand Side
MCG	MagnetoCardioGraphy
MEG	MagnetoEncephaloGraphy
MEMS	Micro Electro-Mechanical Systems
MZI	Mach-Zehnder Interferometer
NIR	Near InfraRed
NV	Nitrogen-Vacancy
OPA	Optical Parametric Amplifier
OPG	Optically-Pumped Gradiometer
OPM	Optically-Pumped Magnetometer
OPO	Optical Parametric Oscillator
PBS	Polarizing Beam-Splitter
PDH	Pound-Drever-Hall
PI	Proportional plus Integrating
PN	Projection Noise
PPKTP	Periodically Poled Potassium Titanyl Phosphate
PSD	Power-Spectral Density
PSN	Photon Shot Noise
PSR	Polarization Self-Rotation
QND	Quantum non-demolition
RF	Radio-Frequency
RHS	Right-Hand Side
SD	Spin-Destruction
SE	Spin-Exchange
SERF	Spin Exchange Relaxation-Free
SNR	Signal-to-Noise Ratio
SNS	Spin Noise Spectroscopy
SOA	State-Of-the-Art
SPN	Spin Projection Noise

Contents

1 Overview / Executive summary

This document reviews the opportunities and plans for quantum enhancement of OPM sensitivity within the macQsimal project. We first survey quantum enhancement techniques that have been developed in the context of other applications such as optical interferometry for gravitational wave detection and atomic clocks. We then describe existing and potential applications of these techniques to quantum enhancement of OPMs. We discuss challenges specific to quantum enhancement of atomic sensors with particular attention to high-sensitivity OPMs. We identify important open questions that condition the utility of quantum enhancement in practical OPM scenarios: the utility of squeezing in optimized instruments, and the compatibility of squeezing techniques with the strongly-interacting media found in high-sensitivity OPMs. Finally, we describe two technologies for quantum enhanced OPMs being developed within macQsimal WP4, and one supporting research activity. The technologies are 1) a sub-pT/Hz$^{1/2}$ OPM with squeezed light probing to operate beyond the photon shot-noise level and 2) a cavity-QED enhanced OPM with sub-mm^3 interaction volume to study measurement-induced spin squeezing. The supporting activity studies the possibility of generating spin squeezing in high-density SERF-regime atomic vapors.

2 Survey of existing quantum enhancement techniques

Quantum sensitivity enhancement was first discussed in the 1960s, and has been intensively studied as one of the main topics of quantum optics since the early 1980s. This work has largely focused on optical interferometry, of interest for gravitational-wave (GW) detection, and atomic clocks. Because an OPM combines a persistent atomic system with an optical readout, many of the techniques developed for either the purely-optical GW application or the purely-atomic clock application are relevant to OPMs.

2.1 History and definitions

Since the pioneering work of Braginsky [1] and Helstrom [2], it has been understood that quantum mechanical noise sources in sensors will determine the ultimate sensitivity in measurement of classical quantities such as displacements or low-frequency magnetic fields. Braginsky noted the importance of noise introduced by the measurement itself and showed that properly-designed measurements, called ”quantum non-demolition” (QND) or “back-action evading” (BAE) could avoid this excess noise source [3]. Helstrom provided a formal theory of quantum measurement applied to quantum systems subject to unknown influences (such as fields). In recent years this approach has become an important subject of study in quantum information, known by the name “quantum metrology” [4]. The use of specially-prepared “squeezed states” with quantum noise below the normal levels was proposed by Caves [5] in the context of gravitational wave detection, and the successful use of squeezed states in interferometric gravitational wave detectors such as GEO600, LIGO and VIRGO [6, 7] has shown that the technique can provide a real-world benefit in demanding applications.

Optically pumped magnetometers have fundamental quantum noise in two elements of the OPM: photon shot noise (PSN) associated with the probe light and the atomic shot noise (ASN) or “projection noise” (PN) associated with the atomic spin ensemble. These are closely related to the concept of the standard quantum limit (SQL). Despite being a central concept in quantum sensing, the SQL has at least three definitions, which coincide in some but not all scenarios.

As concerns the Braginsky approach and BAE measurements, the SQL is the quantum noise level in a naïve but technically perfect measurement. I.e., the noise level that would be observed in a measurement that had no sources of excess noise, and employed the “naïve” measurement strategy of continuous monitoring, with consequent back-action noise.

As concerns the Helstrom approach, the SQL is the noise level when the sensor uses a naïve but technically perfect state. For example, in the context of optical measurements, the SQL would be the PSN present in the output of an ideal laser with no excess noise. A squeezed state is a state with noise in some observable below the corresponding SQL. This definition applies equally to optical states as to so-called spin-squeezed states [8, 9], which are spin states of atomic ensembles with spin noise below the ASN level.

As first shown by Sørensen et al. [10] and extended by many others [11], spin squeezing is only possible when at least some of the atoms are entangled. For this reason, in quantum information contexts the SQL is often taken to be the minimum noise level possible with fully-separable states, such that a noise level below the SQL indicates entanglement.

A sensor can thus have sensitivity beyond the SQL in at least two ways: by outperforming a naïve continuous measurement, or by employing squeezed states. The latter may be squeezed states of light or squeezed states of atoms, a.k.a. "spin squeezed states." The two approaches are in fact closely linked, because QND measurement of a spin ensemble is often employed to produce spin-squeezed states [12-14], and squeezed states of light are predicted to improve the performance of optical QND measurements. For the purposes of this document, we will use the term "Quantum enhancement" to indicate any combination of back-action evasion and use of metrologically relevant squeezed states that improves sensitivity.

2.2 Quantum noise in atomic sensors

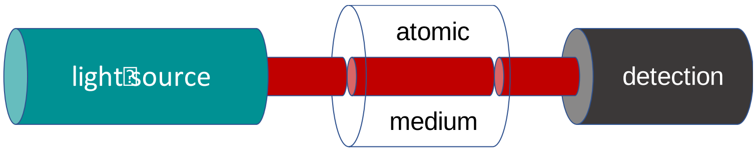

Figure 1: Components of an atomic sensor.

An atomic sensor typically consists of an atomic system and optical auxiliary systems for preparation and detection of the atomic state. Considering only the atomic component, a great variety of atomic systems have been developed as sensors, including gases, vapors, liquids, laser-cooled gases, Bose-Einstein condensates, and atoms dispersed in solid matrices. The optical methods for preparing and measuring the states of the atomic system are also quite varied, and include optical pumping, spin-exchange optical pumping, dispersive and absorptive readout in many geometrical and temporal variations. Quantum enhancement has been studied in very few of these geometries, and is difficult to make generalizations about the potential of quantum enhancement. Nonetheless, a few canonical models have emerged for thinking about the role of quantum noise in atomic sensors [15].

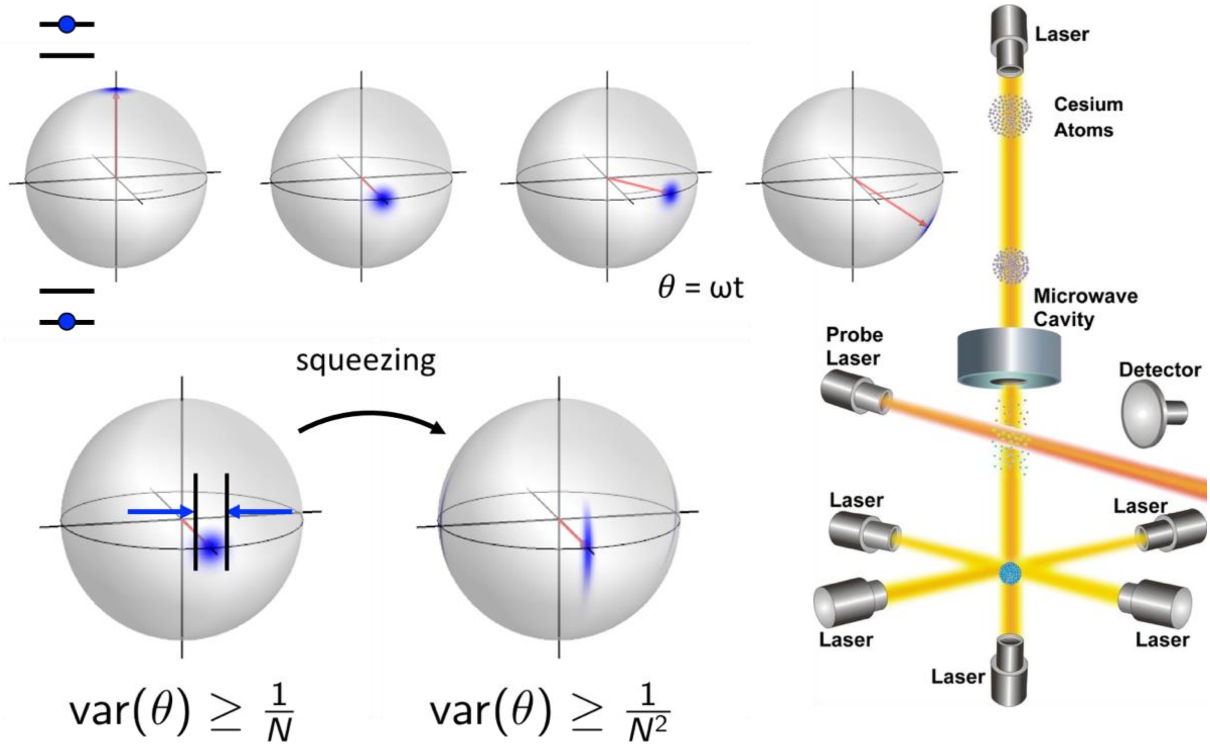

Figure 2: Schematic of a prototypical quantum sensing protocol with two level atoms in a Ramsey interferometer. Diffuse blue represents the statistical distribution of a pure quantum state on the Bloch sphere as it proceeds through different stages of the interferometry. Squeezed states have reduced uncertainty in one or more components.

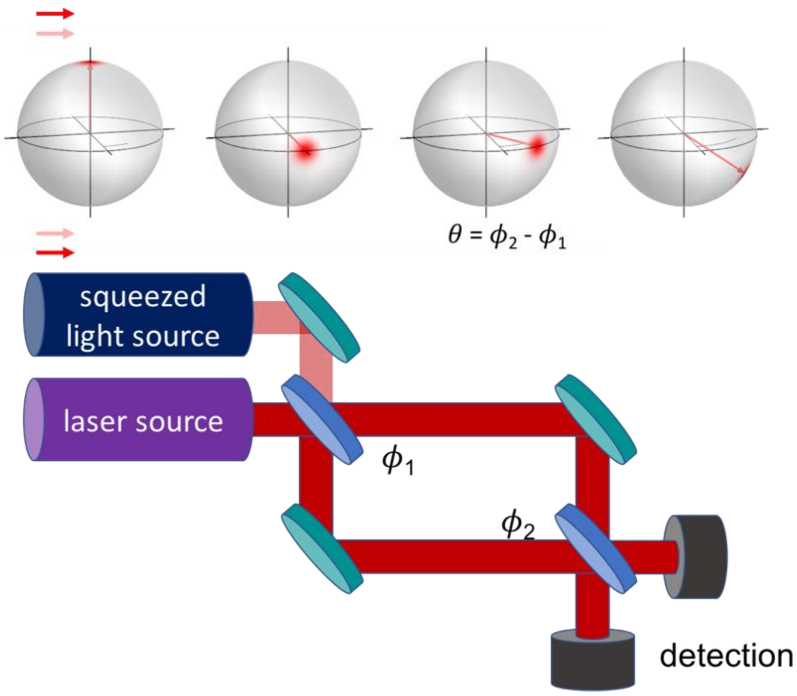

Figure 3: Schematic representation of interferometry in the Bloch sphere representation. The injection of squeezed vacuum into the "dark port" of the first beamsplitter produces a squeezed state of the light in the two arms of the interferometer, in analogy to the spin-squeezed state illustrated in Figure 2.

Much of the prior work on quantum enhanced sensing concerns sensors with only a single component contributing quantum noise [16]. For example, in an atomic fountain clock, see Figure 2, the atomic projection noise can be limiting, and can in principle be improved by spin squeezing. In an optical interferometer, see Figure 3, the quantum noise of the light (photon shot noise) may be important, but quantum noise in other components, in particular quantum noise of the mirrors and other macroscopic objects that determine the optical path and thus the interference condition, is typically negligible. In both of these applications, the quantum system, consisting either of atoms or photons, is first prepared, then experiences a transformation such as a phase evolution, and is then destructively detected. Further measurement repeats the cycle beginning with the preparation of a new ensemble of particles.

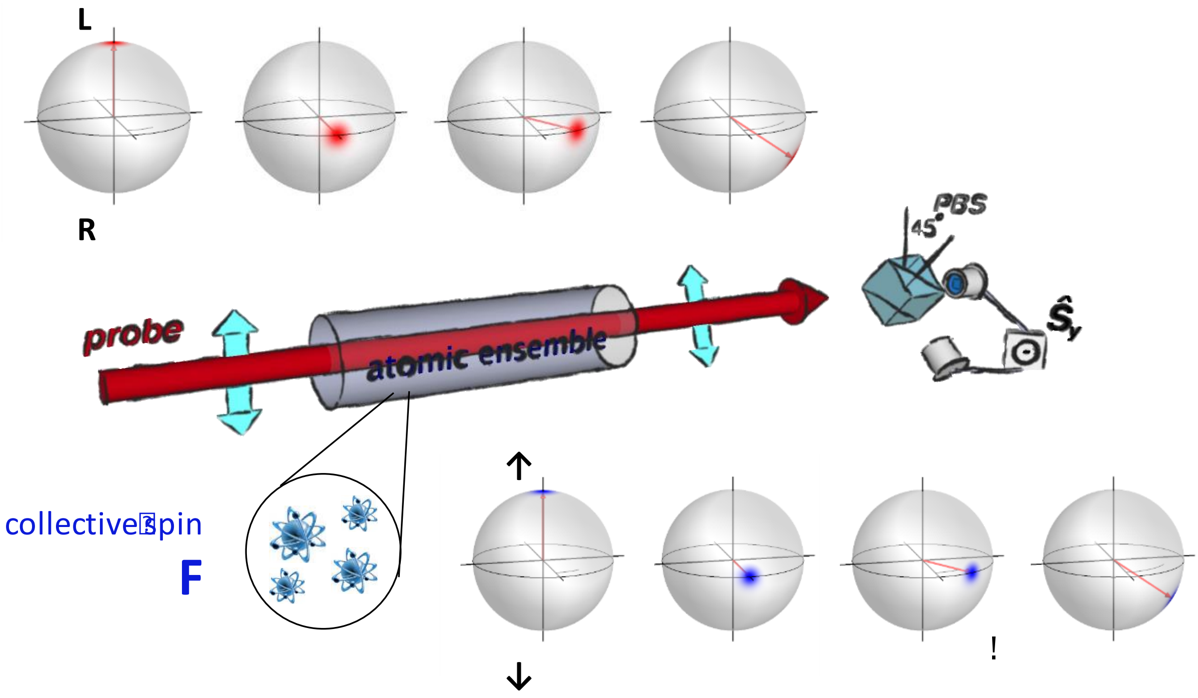

Figure 4: Schematic representation of an OPM operating by Faraday rotation. Centre: A linearly-polarized probe beam passes through an atomic ensemble and experiences a rotation of its plane of polarization by and angle proportional to F_z, the projection of the collective spin of the ensemble along the beam axis. The atomic spin signal and quantum noise (lower row of spheres, with ↑ and ↓ representing spin states) can be understood by analogy with the atomic clock states illustrated in Figure 2. The optical rotation (upper row of spheres, with L and R representing left and right circular polarization) can be understood by analogy with the optical interferometer illustrated in Figure 3. Because quantum noise affects both the atomic and optical components of the OPM, there are two opportunities for quantum enhancement.

In contrast, an OPM typically re-uses the atomic component, both the atomic material *per se* and the quantum state, which is typically neither deterministically prepared, nor destructively measured. Rather, the state is continually pushed toward a state of significant polarization by optical pumping, and continuously but non-destructively read out by an optical probe. An elementary consequence of this is that the OPM contains two quantum systems (atoms and photons) in interaction, and both ASN and PSN can play a role in determining the sensitivity, as illustrated in Figure 4.

This two-system character of the OPM provides opportunities both for quantum sensitivity enhancement using optical squeezing, in instruments where PSN is an important contribution, and spin squeezing, in instruments for which ASN is important. As a general rule, the smaller the number of particles involved, the more important is the quantum noise. For this reason, atomic quantum noise is expected to become more important for miniaturized sensor volumes, and optical quantum noise more important in scenarios of low probe power.

Spin squeezed states were first proposed for spectroscopy and atomic clocks [9]. QND measurement was first proposed in the context of mechanical oscillators [3] being used at the time for gravitational wave detection.

2.3 Quantum enhanced measurement with squeezed light

Caves [5] first noted the role of quantum vacuum fluctuations in determining the noise in an optical interferometer and proposed methods to reduce this noise using squeezed states. His central insight was that in an interferometer of the sort then being considered for gravitational-wave detection (what would become the LIGO GW detectors), what appears as "shot noise" due to the discrete arrivals of uncorrelated particles (photons), can equally and more usefully be described in terms of noise properties of fields. In these interferometers, the detector receives a strong input from a laser, which interferes with a weak and noisy contribution from quantum fluctuations in other modes of the field. When those other modes are in the state of quantum vacuum, the vacuum fluctuations, interfering against the laser field, produce a noisy signal with all the noise properties (including the strength and the "white" spectrum) of the shot noise model. Unlike the shot-noise model, Caves' analysis allows for squeezed states, which have fluctuations below the vacuum state level. When these interfere with the laser's contribution, the result is a signal with noise levels below the shot noise level.

The practicality of squeezed light enhancement in applications is clearly demonstrated by the gravitational wave detectors GEO600 [7], LIGO [17] and VIRGO [18], all of which have employed and continue to employ squeezed light to boost sensitivity.

The same insights apply to a wide variety of interferometers, as well as to basic detection strategies such as homodyne detection. Of particular interest to OPMs based on polarization rotation, a polarization rotation measurement using balanced detection is analogous to a Mach-Zehnder interferometer (MZI), and the Caves analysis applies directly.

2.3.1.1 Physical processes to produce optical squeezing

Several nonlinear optical processes have been demonstrated to reduce PSN below the shot noise level. These include parametric amplification by three-wave mixing, parametric amplification by four-wave mixing, two-photon absorption, optical Kerr nonlinearity, and optical self-rotation. Despite an intensive study of such processes in the 1980s, following Caves' proposal for improvement of gravitational wave detection with squeezed light [5], the earliest-demonstrated processes remain the most commonly used.

Parametric amplification with three-wave mixing [19] employs a short-wavelength pump laser and a $\chi^{(2)}$nonlinearity, typically from a non-centrosymmetric crystal. In the most common, "single-mode squeezing" scenario, the pump frequency $\omega_p = 2\omega$ is the second harmonic of ω, the frequency to be amplified. In this scenario, the parametric process produces an amplification of one quadrature amplitude and de-amplification of the other quadrature amplitude. When fed with vacuum, which has equal noise in each quadrature, the output has one quadrature with noise below the vacuum noise level, which is also the SQL, as ideal lasers and vacuum have the same quadrature noise level.

The $\chi^{(2)}$ parametric amplification can be produced in a crystal that is transparent to both ω and 2ω, and introduces very little excess noise. The achievable squeezing is then limited by losses in the parametric amplification optics and any other losses prior to photo-detection. In the context of gravitational-wave detection, squeezing of up to 15 dB below the SQL [20] have been demonstrated at 1064 nm. With proper choice of crystal, quadrature squeezing can be produces by this method at a very broad range of optical frequencies. In particular, such squeezed light sources are tunable, which allows them to be matched in frequency to the lasers of existing instruments, e.g. in gravitational-wave detection, or tuned to any desired point relative to an atomic line. It should be noted, however, that lower degrees of squeezing have been demonstrated at shorter wavelengths, e.g. 5.6 dB of quadrature squeezing at 795 nm [21, 22].

Parametric amplification with four-wave mixing [23] employs a pump laser and a $\chi^{(3)}$nonlinearity. In atomic sensing contexts, atomic media (warm vapors, laser-cooled atoms, atomic beams) have been used as nonlinear media for their extremely large $\chi^{(3)}$nonlinearities. In other contexts, squeezing by four-wave mixing has been produced in optical fibres using short-pulse lasers and the $\chi^{(3)}$nonlinearity of the silica fibre itself. Experiments with hot vapors have demonstrated high degrees of relative-intensity squeezing [24] and moderate relative-intensity squeezing at frequencies below 10 Hz [25]. It is also possible to produce quadrature squeezing in this way [26], but the degree of squeezing is not large. It should be noted that when implemented in an alkali vapor, the technique is only effective at a particular frequency within the Doppler-broadened spectrum of the D_1 line.

Another squeezing technique developed in hot vapors is polarization self-rotation (PSR). This is also a four-wave mixing technique that employs the strong resonant $\chi^{(3)}$nonlinearity available with atomic media. As with other atomic $\chi^{(3)}$ processes it can be produced at low optical power, and is limited to a narrow range of optical frequencies. In contrast to the works just described, PSR employs a single beam, and induces correlations between the minority Stokes parameters of the beam. For example, a horizontally-polarized beam will have large S1, and only quantum fluctuations in S2 and S3. After the PSR process, the fluctuations in S2 and S3 will be correlated, in such a way that a linear combination of these, e.g. $(S1 + S2)/\sqrt{2}$, will be squeezed [27-29]. Unfortunately, as with quadrature squeezing by FWM in vapors, the degree of squeezing producible in this way appears to be limited.

2.3.1.2 Cavity enhancement

For weak optical nonlinearities, optical resonators are commonly employed to allow the light of interest to pass multiple times through the nonlinear optical medium, and thereby experience a stronger nonlinear effect, leading to stronger squeezing. Such devices, consisting of an optical resonator around a nonlinear optical medium producing parametric amplification, is an optical parametric amplifier (OPA), also called a sub-threshold optical parametric oscillator (OPO). Squeezing is highly sensitive to losses, and any loss within the resonator is, like the nonlinear optical effect, experienced multiple times by the resonated light fields. For this reason, the achievable squeezing in cavities is highly dependent on the quality of mirror surfaces and coatings, as well as anti-reflection coatings on the surfaces of any transparent elements inside the resonator.

2.3.1.3 Monolithic and semi-monolithic cavities

For squeezing at NIR wavelengths, the principal limitations are losses in the OPA cavity and the relatively low gain of nonlinear optical materials that are transparent at the shorter atom-resonant wavelengths. Low gain can be fully compensated by higher pump power with a correspondingly higher cost and complexity. To reduce intra-cavity losses to the minimum (intrinsic losses in the nonlinear materials), monolithic OPA designs have been developed [30, 31], but to date are not widely employed. So-called “semi-monolithic” designs, in which one face of the crystal is used as a mirror surface while the other is anti-reflection coated, are nonetheless widely employed.

2.3.1.4 Generation of polarization-squeezed light

Many OPMs strategies employ optical polarization rotation and balanced detection as a means to observe atomic spin precession. In these OPMs, the detected optical variable is a Stokes parameter, and it is natural to ask whether Stokes parameters can be squeezed. As noted in Section 2.3.1.1, PSR is a process that naturally produces small amounts of polarization squeezing at specific frequencies. A more versatile method is to combine quadrature squeezed vacuum of one polarization with a coherent state (laser output) of the orthogonal polarization [32-34]. Both methods have been applied for quantum-enhancement of OPM sensitivity [35], [36].

2.4 Spin squeezing

It was first understood in the context of ion-trap spectroscopy that spin-squeezed states can be used to reduce atomic shot noise [8, 9]. In many ways, the analogy to optical squeezing is surprisingly close, considering that light is described by an infinite-dimensional quantum field, whereas the internal state of a collection of atoms is described by a finite-dimensional quantum-mechanical wave function. One central insight is the existence of generalized uncertainty principles for spin components. Starting with the commutation relations for spin components $[J_x, J_y] = i\, J_z$ and cyclic permutations, the Robertson-Schrodinger relation $\delta A\ \delta B \geq \frac{1}{2}\ |\langle [A, B] \rangle|$, where A and B are quantum mechanical observables, implies an uncertainty relation $\delta J_x\ \delta J_y \geq \frac{1}{2}\ |\langle J_z \rangle|$ and cyclic permutations. This is analogous to the uncertainty relation $\delta X\ \delta P \geq \frac{1}{2}$ that constrains the uncertainties (and hence the noise) of optical quadrature amplitudes X and P for any given mode of the optical field. We consider, for example, a fully-polarized state of N spin-1/2 atoms, known in the context of spin squeezing as a coherent spin state (CSS). If this state is polarized along the Z direction, so that $\langle J_z \rangle = N/2$, then the uncertainty relation reads $\delta J_x\ \delta J_y \geq N/4$. Indeed, the fully-polarized state saturates this inequality, as $\delta J_x = \delta J_y = \sqrt{N}/2$, with the consequence that the angular uncertainty is $\delta\theta = \delta J_x / \langle J_z \rangle = 1/\sqrt{N}$. This defines the SQL for a spin-based measurement using rotation on the Bloch sphere. This “atomic shot noise” level can be surpassed, as there exist states with uncertainty $\delta\theta = \delta J_x / \langle J_z \rangle$ below this level. Such states are said to be squeezed by the Wineland criterion, which concerns the angular uncertainty, and not the spin component uncertainty *per se*.

Spin squeezing concepts can of course be applied not only to true spins, but also to pseudo-spins, which may be defined with reference to sets of discrete states available to a bosonic system. For example, considering two possible states L and R, which might be occupancy of the left and right wells of a double well potential, we can define

$$J_x = \frac{1}{2}\left(a_L^\dagger a_R + a_R^\dagger a_L\right) \qquad \textit{Eq. 1}$$

$$J_y = \frac{i}{2}\left(a_L^\dagger a_R - a_R^\dagger a_L\right) \qquad \textit{Eq. 2}$$

$$J_z = \frac{1}{2}\left(a_R^\dagger a_R - a_L^\dagger a_L\right) \qquad \textit{Eq. 3}$$

where a_L, a_R indicate annihilation operators for the left and right wells, respectively. We see that these satisfy $[J_x, J_y] = i\, J_z$ and cyclic permutations, and thus will have the same uncertainty relations as a real spin system. In the same way, pseudo-spin operators can be defined for identical bosons in any pair of states.

2.4.1 Generation of spin squeezing by coherent dynamics

As described above, optical squeezing is achieved by nonlinear optical processes, which is to say by interactions among photons. It is natural to expect that spin squeezing can also be produced in this way. Indeed, coherent dynamics have been exploited to produce spin squeezing in two distinct scenarios: in Bose-Einstein condensates [37-40], where coherent interactions can be produced by ultra-cold collisions, and in cavity-QED setups, in which atoms interacting with the same field mode can experience an effective interaction [41, 42]. This latter scenario is referred to as “cavity squeezing.”

2.4.1.1 Dynamical spin squeezing by coherent collisions in BECs

For example, atoms of a single species in a double-well potential can be described by the Hamiltonian

$$H_{DW} = \kappa(a_L^\dagger a_R + a_R^\dagger a_L) + c(a_L^\dagger a_L^\dagger a_L a_L + a_R^\dagger a_R^\dagger a_R a_R) \qquad \textit{Eq. 4}$$

where a_L, a_R again indicate annihilation operators for the left and right wells, respectively, κ describes the tunnel coupling, and c describes the collisional energy, $c > 0$ for repulsive interactions. For constant $N \equiv a_L^\dagger a_L + a_R^\dagger a_R$, we find that

$$H_{DW} = 2\kappa J_x + 2cJ_z^2 + \text{const.} \qquad \textit{Eq. 5}$$

For $c > 0$, the ground state of this system is the one that minimizes a linear combination of the inter-well coherence J_x and the number difference variance $\delta J_z^2 = \langle J_z^2 \rangle - \langle J_z \rangle^2$ (note that by symmetry the ground state will have $\langle J_z \rangle = 0$). For this case, we see that simply cooling to the ground state in this scenario will produce a squeezed state satisfying the Wineland criterion.

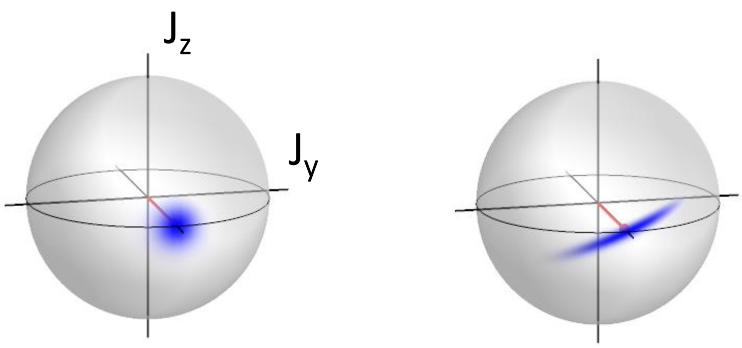

Figure 5: Spin squeezing by the single-axis twisting Hamiltonian.

Other methods to generate squeezing with ultracold collisions employ specific Hamiltonians to evolve from a fiducial initial state to a desired squeezed state. For example, the so-called “single-axis twisting” Hamiltonian

$$H_{OAT} = \alpha J_z^2 \qquad \textit{Eq. 6}$$

Can be generated from Eq. 5 by setting $\kappa = 0$. As shown in Figure 5, this produces a shearing of the uncertainty distribution on the Bloch sphere describing the pseudo-spin, and converts easily-prepared spin coherent states to spin-squeezed states.

BEC squeezed states have been used for quantum enhancement in interferometric sensing [43, 44], although to date BEC sensors themselves have not found practical applications, in part due to the complexity of the experimental apparatus necessary to produce them.

2.4.1.2 Dynamical spin squeezing by cavity-mediated interactions

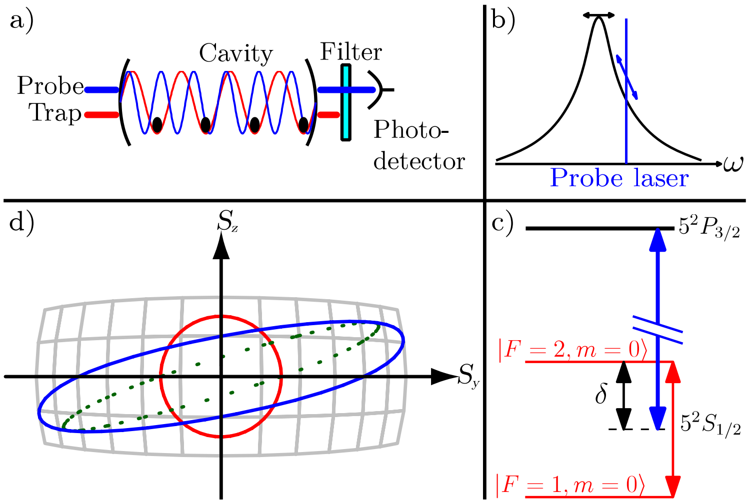

Figure 6: Spin squeezing by cavity-mediated interactions. Figure from [41]. The coupling laser ("Probe", blue in figure) is tuned to a frequency that is simultaneously red- (blue-)detuned from the F=1 (F=2) ground hyperfine state, and blue detuned from the cavity resonance. In this configuration, the circulating power in the cavity P_{cav} is linear in the atom number difference $J_z = \frac{1}{2}(n_2 - n_1)$. At the same time, the light shift on the F=1 (F=2) state is negative (positive), described by a term in the Hamiltonian $H_{cav} \propto P_{cav}J_z \propto J_z^2$. In this way, the driven cavity creates an effective pairwise interaction among the atoms, leading to the same dynamics and squeezing illustrated in Figure 5.

In proper conditions, a driven optical cavity can create an effective two-body interaction among atoms coupled to the cavity mode. This is illustrated in Figure 6. The resulting spin dynamics strongly resemble what can be produced with ultra-cold collisions, but does not require quantum degeneracy. The achievable squeezing does, however, strongly depend on the uniformity of the coupling to the cavity mode, and the highest performing experiments to date have used cold atoms confined to optical lattices with periods commensurate to the period of the cavity mode, e.g. a lattice with spacing of ½ 1560 nm for a cavity mode with spacing ½ 780 nm [42, 45].

2.4.2 Generation of spin squeezing by non-destructive measurement

Precise, non-destructive measurement of an atomic system provides another method of generating spin squeezing. OPM technologies often include a precision measurement of the atomic system, and in many cases, this is also a non-destructive measurement. As a result, some OPM techniques appear likely to generate and benefit from spin squeezing without any special modification. Measurement-induced squeezing has been extensively studied in model systems [13, 45-49] and explored in the context of DC magnetometry in cold atoms [48] and RF magnetometry in vapors [50-52] and cold atoms [53].

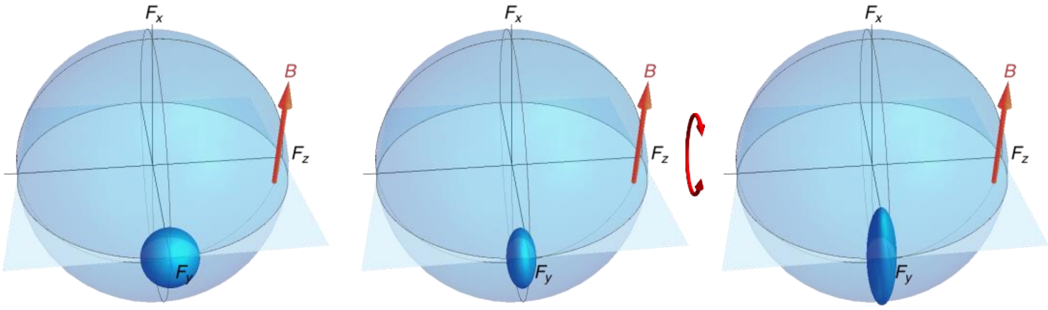

Figure 7: illustration of non-destructive measurement effects on the quantum uncertainty of a spin state, where the collective spin is F. The initial state (left panel) describes a state fully polarized along y, with an isotropic spin uncertainty distribution. The optical measurement provides information about F_z, reducing its uncertainty (middle panel). The accompanying measurement back-action causes a small random rotation about the F_z axis, increasing the uncertainty of F_x (right panel).

In the spirit of the Faraday rotation measurement illustrated in Figure 4, we consider an interaction by which the Stokes parameters (S_x, S_y) are rotated by and angle $\phi = G\,J_z$. To have a simple quantum mechanical model for this, we can consider a pulse of light, and define the Stokes operators

$$S_x = \frac{1}{2}\left(a_L^\dagger a_R + a_R^\dagger a_L\right) \qquad \textit{Eq. 7}$$

$$S_y = \frac{i}{2}\left(a_L^\dagger a_R - a_R^\dagger a_L\right) \qquad \textit{Eq. 8}$$

$$S_z = \frac{1}{2}\left(a_R^\dagger a_R - a_L^\dagger a_L\right) \qquad \textit{Eq. 9}$$

where a_L, a_R are now annihilation operators for left- and right-circularly polarized photons, respectively. Clearly, these also obey angular-momentum commutation relations $[S_x, S_y] = iS_z$ and cyclic permutations. For small ϕ the polarization rotation can be described by the input-output relation

$$S_y^{out} = S_y^{in} + G\,S_x^{in}\,J_z^{in}. \qquad \textit{Eq. 10}$$

The LHS is directly observable, for example with a polarimeter consisting of polarization optics and differential photo-detection as shown in Figure 4. The first term on the RHS is the input value of the Stokes operator, which in a classical description and in the usually-adopted balanced condition is zero. The quantum fluctuations of this variable are equivalent to PSN, and this first term is the optical quantum noise contribution to the measured variable. The second term is the signal, proportional to the atomic variable of interest J_z times S_x^{in}, which for a linearly-polarized input is simply the number of photons over two.

This measurement of J_z^{in} has an error variance of

$$\mathrm{var}(J_z)_{meas} = G^{-2} S_x^{-2} \mathrm{var}(S_y^{in}) \qquad \textit{Eq. 11}$$

and thus, results in a post-measurement state with variance

$$\mathrm{var}\left(J_z^{out} | S_y^{out}\right) = \frac{1}{1/\mathrm{var}\left(J_z^{in}\right) + G^2 S_x^2 / \mathrm{var}\left(S_y^{in}\right)} + N_{meas} \qquad \textit{Eq. 12}$$

Where $\boldsymbol{N_{meas}}$ is any excess noise contributed by the measurement, for example due to incoherent scattering of photons. In contrast to what happens with dynamical squeezing, this is a conditional variance: it describes the remaining uncertainty when one knows the outcome of the measurement. The measurement has, in colloquial language, "collapsed" the system to a state with smaller uncertainty.

If the uncertainty relations are to be preserved, this reduction of uncertainty in J_z is necessarily accompanied by an increase of uncertainty in J_x, due to the commutation relation $[J_z, J_x] = iJ_y$. That is, accompanying the effect of atoms on the light, which makes possible the measurement, there must also be a "measurement back-action", i.e., a dynamical effect of the light on the atoms. To understand this, we note that Eq. 10 can be derived as the action of a Hamiltonian

$$H_{FR} = S_z J_z \qquad \textit{Eq. 13}$$

which acts for a time $G/\hbar$. Computing the effect on J_y (again in the regime of small rotations), we find

$$J_x^{out} = J_x^{in} + G\, J_y^{in}\, S_z^{in}. \qquad \textit{Eq. 14}$$

We note that this contains S_z^{in}, which for the linearly-polarized input we are considering has zero mean and a variance determined by PSN. We see that the same interaction that decreases reduces uncertainty of J_z increases the uncertainty of J_x as required to preserve the spin uncertainty relations.

2.4.3 Effect of repeated non-destructive measurement

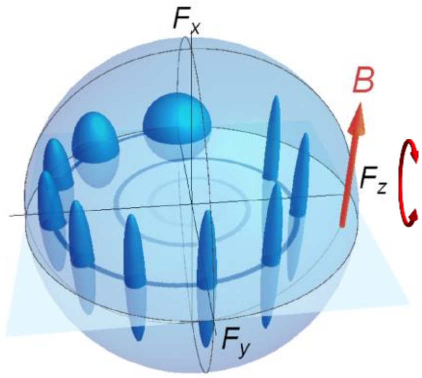

Figure 8: Evolution of the spin uncertainty for a spin state precessing about a B-field along the x-direction, when subjected to repeated non-destructive probing of the F_z spin component. The measurement back action, a sequence of random rotations about the F_z direction put uncertainty into the F_x component, while the measurement reduces uncertainty in both the F_z and F_y components, allowing greater precision in determining both the evolution of the azimuthal angle and the amplitude.

A number of OPM strategies, including Bell-Bloom and FID subject the spins to repeated non-destructive measurement as the spins precess. This scenario has been studied with cold atoms [14, 54], and shows the interesting behaviour that the spin state uncertainty is reduced in both the radial and azimuthal directions, see Figure 8. As the spins precess, the signal is determined by these two components in linear combination, but the out-of-plane component, which becomes uncertain due to measurement back-action, has no effect on the measurement. This interestingly represents a scenario in which continuous QND measurement, as it would be normally applied in an OPM, potentially leads to significant quantum enhancement without side effects due to measurement back-action.

3 Challenges and open questions

3.1 Quantum enhancement of optimized atomic sensors

Due to uncertainty relations, squeezing of one variable inevitably introduces additional noise into another variable. Similarly, back-action evading techniques necessarily limit the scope of a measurement, in order to avoid introducing back-action noise into the measurement record. While it is clear that these trade-offs are beneficial in model scenarios, and even in the relatively simple in-practice scenarios encountered in gravitational-wave detection [7, 17], it remains to be shown that these quantum enhancement techniques are beneficial under optimized conditions for a system as complex as an OPM, in which an atomic and optical system interact.

The importance of this point should not be understated: if quantum enhancement provides an advantage under some operating conditions, but not at the optimum operating point, then traditional methods, normally simpler to implement than quantum enhancement, will be at least as effective as quantum enhancement at improving the sensitivity.

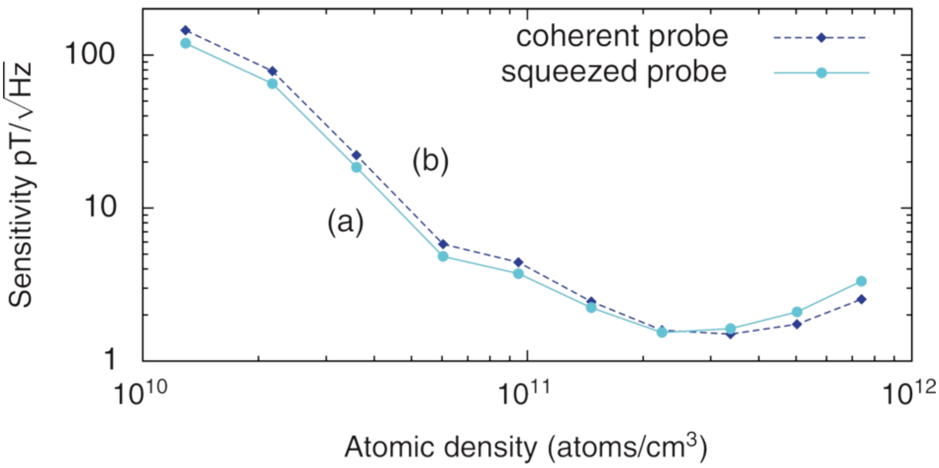

Figure 9: Effect of polarization squeezing on a single-beam magnetometer's sensitivity. Figure from [35].

An important illustration of this point is shown in Figure 9, taken from [35]. That work implemented a single-beam OPM with pT/rtHz sensitivity and a single-beam squeezer operating by polarization self-rotation. They found that the use of squeezed light in their OPM improved magnetometer sensitivity at low atomic densities, but worsened it at higher atomic densities. At the optimal atomic density, the sensitivity was unchanged (to within experimental precision) by the application of squeezed light. The cause of this response to squeezed light could not be determined in that experiment. Because atom number density is typically an adjustable parameter used to optimize sensitivity, this provides an example in which quantum enhancement by squeezed light is of limited utility, despite providing some advantage in some range of parameter values.

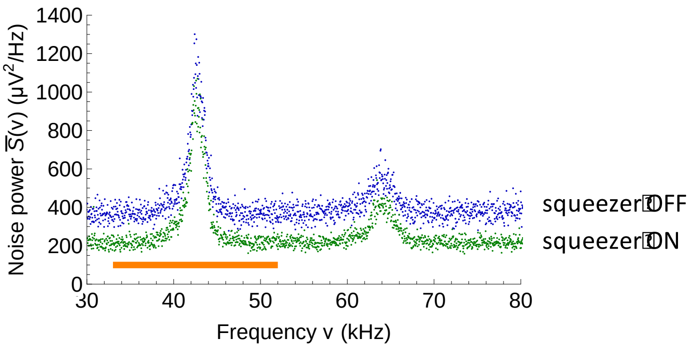

Figure 10: Spin noise spectra (SNS) with and without quantum enhancement by polarization squeezing. Stronger and weaker peaks correspond to ^{85}Rb and ^{87}Rb, respectively, and rise from a white shot-noise background. The effect of the squeezing is to reduce the background, which makes the SNS more visible. Relevant features of the SNS peaks are the centre frequency ν_L and the linewidth $\Delta\nu$.

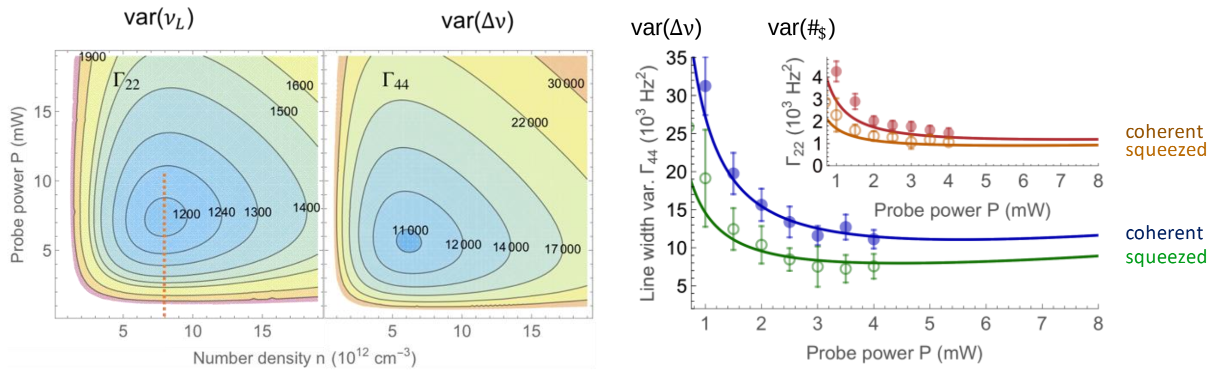

Figure 11: Quantum advantage in SNS under optimized conditions. Figures from [55]. Left panel shows model-derived sensitivities (variances in the maximum-likelihood estimator) for the line centre ν_L and linewidth $\Delta\nu$ as a function of number density and probe power. In both cases a global optimum can be identified, which indicates a best sensitivity for the measurement using any classical resources. Red vertical line shows the range of parameters studied in the right panel. Right panel compares theoretical sensitivity and measured sensitivity with and without squeezed light.

More detailed studies of the role of quantum noise and quantum enhancement in number-optimized measurements have been carried out for spin-noise spectroscopy (SNS) in atomic vapors [55, 56]. The SNS application is of interest in other domains because it provides a minimally-perturbative measurement of spin parameters such as relaxation rates [57]. Here it is interesting because it contains the same quantum noise elements as an OPM, while also being quantum noise limited under a broader range of conditions. As shown in Figure 10 and Figure 11, when SNS is used to identify the precession frequency ν_L and linewidth $\Delta\nu$, globally-optimum values for the atom number density and probe power can be identified. Operation with polarization-squeezed light, generated in a $\chi^{(2)}$ OPA, the sensitivity to both parameters could be improved beyond the best-possible sensitivities with only classical resources. This gives some reassurance that quantum enhancement with squeezed light will be useful in optimized OPMs as well.

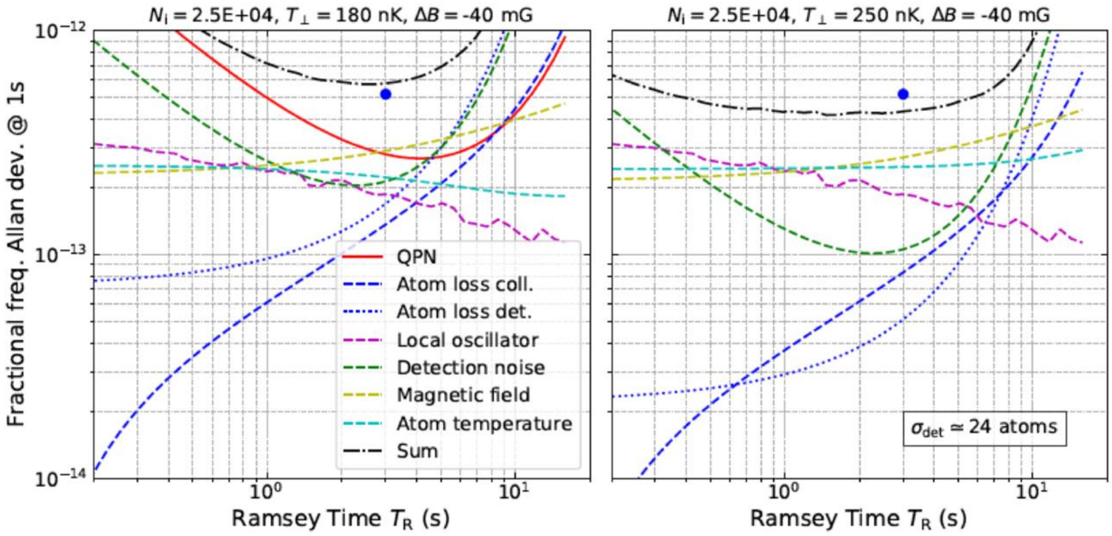

Figure 12: Noise budget of a compact microwave clock with and without spin squeezing. Figure from [58]. Left panel shows short-term stability noise budget without squeezing protocol, right panel shows the same with measurement-induced spin squeezing. Blue dot shows experimental optimum with classical operation.

Perhaps the most detailed study to date on the topic of quantum enhancement in optimized instruments comes from the area of atomic clocks. Using a compact microwave clock and spin squeezing by cavity-enhanced non-destructive measurement, a significant reduction in total noise was observed under conditions optimized for short-term stability [58].

3.2 Quantum spin noise in high-density media

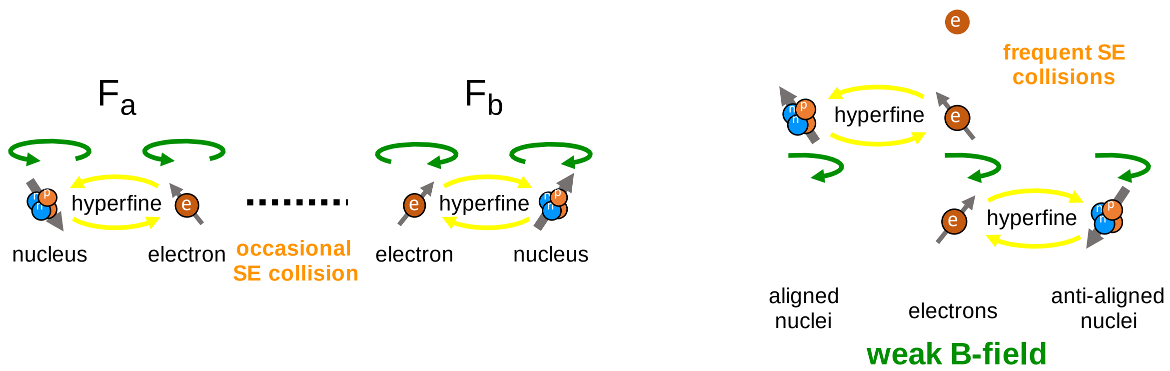

Figure 13: Spin-exchange and SERF regimes in alkali vapors. Left panel illustrates the interactions at low density and high field, the spin-exchange (SE) regime. Frequency scales for hyperfine (HF), Larmor (L), and SE collisions are ordered $\omega_{HF} > \omega_L > \Gamma_{SE}$. The system can be understood as two populations, one in each hyperfine manifold, precessing in opposite directions due to the magnetic field with decoherence produced by infrequency SE collisions. Right panel illustrates the interactions at high density and low field, the spin-exchange-relaxation-free (SERF) regime, where $\omega_{HF} > \Gamma_{SE} > \omega_L$. In this regime, SE collisions pass spin angular momentum among all the atoms in a local region faster than precession can take place. As a result, the entire ensemble precesses at an average rate and the mean spin value does not relax due to SE collisions.

To date, nearly all spin squeezing experiments have been performed with weakly-interacting atomic media, most often with cold and ultra-cold atoms. In the few cases in which atomic vapors have been used [51, 52, 59, 60], relatively low densities were employed. In contrast, the highest-sensitivity magnetometers use high-density vapors in the SERF regime. Low-density vapors can be accurately modelled by considering at most two-atom effects, i.e. by including the single-atom interaction with the field, optical beams, and environment, as well as the two-atom spin-exchange interaction taken as a decoherence mechanism, see Figure 13 (left). In contrast, spin-exchange effects in the SERF regime occur in a many-atom regime, in which spin polarization and coherence are passed many times from atom to atom within a local region before eventually relaxing due to spin-destruction collisions [61, 62], see Figure 13 (right). It is not obvious that such a complicated many-body system will support the quantum correlations of a spin-squeezed state. The squeezed state is produced by entanglement among the atoms, but entanglement is famously sensitive to decoherence and the random spin-exchange collisions would appear to rapidly increase the entropy of the many-body state. Existing theory to describe the SERF regime [62] is a single-atom mean-field theory. It has been shown to agree with average behaviour of SERF-regime media in experiment, but does not provide a description of correlated atomic behaviour, and as such cannot predict quantum noise properties.

4 Methods for quantum enhancement of OPM sensitivity in macQsimal

In light of the background and status of quantum enhancement of OPMs described above, we can identify specific research targets that will answer important open questions and enable quantum enhanced sensitivity in high-performance OPMs in the future. The first of these (see Section 4.1) is a squeezed-light OPM operating in a regime of simultaneous high sensitivity and quantum-noise-limited performance. The second (see Section 4.3) is an OPM operating either in SERF or FID regime but with greatly reduced active volume and atom number, and thus a greater noise contribution from atomic shot noise. This second activity will enable study difficult questions concerning the use of spin squeezing in OPMs. An associated question (see Section 4.2) is whether spin squeezing can be produced in complex media such as SERF-regime vapors, in which rapid SE collisions share spin angular momentum among many atoms.

4.1 Sub-pT/√Hz OPM enhanced with squeezed light

4.1.1 Overview and goals

This activity will apply squeezed light quantum enhancement to a high-sensitivity OPM operating with a modern and relatively simple operating principle. For this we employ a Bell-Bloom scalar magnetometer [63-65] with off-resonance Faraday rotation readout. We operate in an intermediate density regime, to have high sensitivity without the many-body coherence issues, e.g. SERF, that become important at higher densities. In this regime, the sensitivity is limited by photon shot noise at higher magnetic-field frequencies, and by atomic shot noise at lower magnetic field frequencies, with a transition region between the two regimes at around 500 Hz. This provides an opportunity to study the effect of optical squeezing on both the sensitivity and the bandwidth of the magnetometer, and may also help to understand the role of spin squeezing in continuously-probed OPMs.

4.1.2 Prior work on squeezed-light magnetometers

A squeezed-light enhanced magnetometer was first accomplished in 2010 [36] probing the alignment to orientation conversion (AOC) in a non-polarized ensemble of Rb atoms. This experiment was performed in an area of operating parameters where the photon shot noise was dominant so that the suppression of the photon shot noise was considerable. The sensitivity of the magnetometer was improved by 3.2 dB and reached a value of around $\mathrm{nT}/\sqrt{(\mathrm{Hz})}$ when polarization squeezed light [66] was used for probing. Since then, the most sensitive squeezed light enhanced magnetometer was implemented by Horrom et al. [35], with sensitivity of $2\mathrm{pT}/\sqrt{(\mathrm{Hz})}$. Squeezed light was generated through polarization self-rotation (PSR) in an atomic squeezer, a Rb cell that was placed before magnetometer and along the propagation axis of the probe beam. The performance of the particular magnetometer was limited in lower frequencies due to technical noise in the laser intensity.

4.1.3 High sensitivity shot noise limited Bell Bloom magnetometer

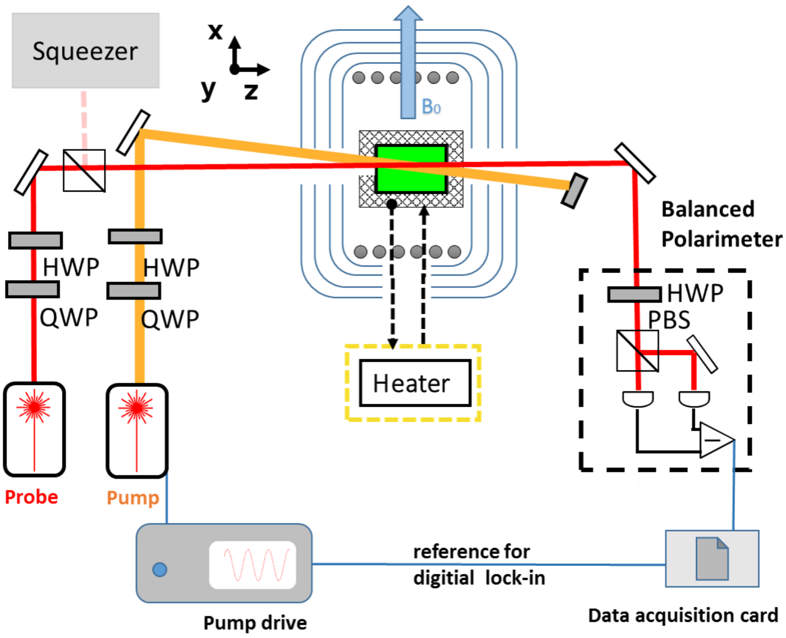

Figure 14: Magnetometer experimental setup.

Figure 14 shows the schematic of the Bell Bloom magnetometer. This scalar atomic magnetometer can measure the absolute value of a magnetic field using a circularly polarized pump beam nearly parallel to the probe beam. We induce the Bell-Bloom excitation of the spin precession around a perpendicular magnetic field by sinusoidally modulating the current of a DFB laser, and therefore changing the detuning of the pump on and out of resonance, synchronously with the Larmor frequency at 10s of kHz. We characterize the amplitude and the decoherence time T_2 of the magnetometer from the free induction decay (FID) part of the signal that is obtained when we turn the pump modulation off. The main part of the signal with the modulation on is demodulated with a lock-in amplifier.

4.1.4 Quantum noise contributions and classical sensitivity

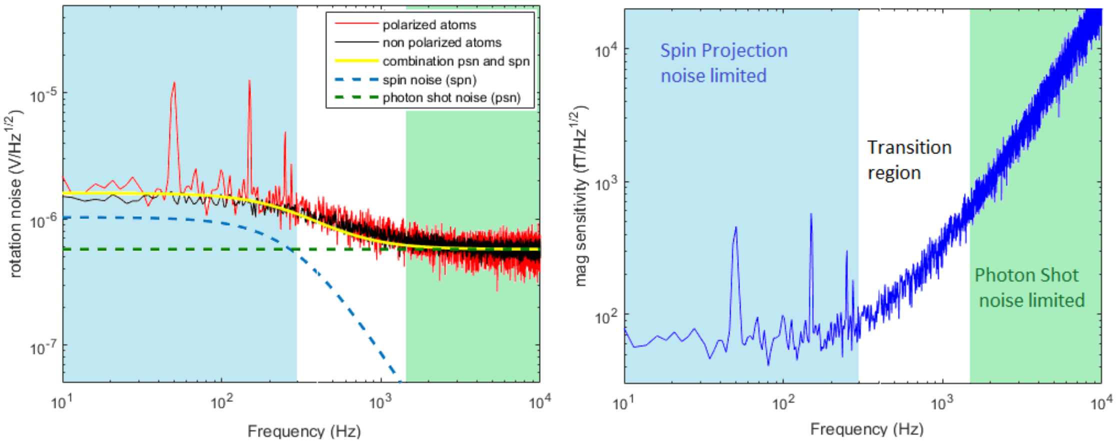

*Figure 15: **a) Noise spectrum of the magnetometer**. Operating the magnetometer with coherent light probing at an ambient field of 4 μT we have managed to identify a regime of minimum technical noise. At these conditions, the atomic spins are driven to precess at 28 kHz, a detection frequency at which the detector is photon shot noise limited. The instruments sensitivity, calculated to be better than 100 $fT/Hz^{1/2}$, classifies our experimental setup as the most sensitive shot noise limited magnetometer amenable for squeezed light application. In quantum noise limited scenario, we can distinguish three regions, defined by range of frequency in which the spin projection noise or the photon shot noise is dominant and a transition region between them. **b) Magnetic sensitivity as a function of frequency.** Shows transition from the projection noise limited to the photon shot noise limited regimes.*

The detection system described above monitors the rotation of the polarization plane of the linearly polarized probe beam by a small angle ϕ, equal to the projection F_z of the collective atomic angular momentum along the probe direction multiplied by a coupling constant G. The signal from the balanced detector is proportional to S_y^{out}, the Stokes parameter after the atomic interaction: $S_y^{out} = S_y^{in} + S_x^{in}\, GF_z$. When quantum noise limited, the power spectral density (PSD) in this signal is

$$\mathrm{PSD}_{S_y^{out}}(\nu) = \mathrm{PSD}_{S_y^{out}}(\nu) + G^2 \langle S_x^{in} \rangle^2\, \mathrm{PSD}_{F_z}(\nu), \qquad \textit{Eq. 15}$$

where we have assumed that the two terms are independent and that the operator S_x^{in} is large enough to be treated as a classical quantity. The photon shot noise shows in the first term of this equation. The impact of the polarization squeezing is to suppress this variance below the standard quantum limit (SQL): $\mathrm{PSD}_{S_y^{out}}(\nu)_{\mathrm{squeezed}} < \mathrm{PSD}_{S_y^{out}}(\nu)_{\mathrm{SQL}}$.

The demodulated signal shows a Lorentzian line shape with detuning of the optical pumping from the Larmor frequency, with the in-phase or 0° component having an “absorptive” or even-symmetry line shape and the quadrature or 90° component having a “dispersive” or odd-symmetry line shape. The 90° component thus provides a signal $\tilde{S}_y$ that is linear in the magnetic field strength, i.e., the scalar magnetometer signal. The noise spectrum of this signal after lock-in amplification is shown in Figure 15 for two conditions: when the pump in on (polarized atoms, red) and off (non-polarized atoms, black). The un-pumped condition provides the reference level for quantum noise, both atomic and optical. When pumped, the noise spectrum shows a very similar behaviour apart from technical noise peaks at the line frequency and harmonics. The observed noise transitions from a PSN-limited regime at frequencies above about 500 Hz, to an ASN-limited regime from 10 Hz – about 500 Hz.

The slope of the dispersive signal is $\partial S/\partial B = A(0)/\Gamma_2$, where $A(0)$ and Γ_2 are the amplitude and width of the dispersive Lorentzian for dc magnetic fields. The frequency-dependent sensitivity is then

$$\delta B(\nu) = \frac{1}{\gamma T_2}\frac{1}{A(\nu)}\delta\tilde{S}_y(\nu), \qquad \textit{Eq. 16}$$

where $\delta\tilde{S}_y(\nu)$ is the observed noise spectrum in the demodulated signal. The responsivity of the magnetometer is

$$A(\nu) = \frac{A(0)}{\sqrt{1+(2\pi\nu T_2)^2}} \qquad \textit{Eq. 17}$$

This accounts for the low-pass filtering produced by the finite relaxation time of the spin polarization. Dividing the noise spectrum with this amplitude response we obtain the sensitivity Eq. 16 which is constant in the spin noise limited regime and increases as photon shot noise becomes dominant.

4.1.5 Generation and detection of polarization squeezed light

For the production of polarization squeezing we use the experimental apparatus that is shown in Figure 16. A squeezed vacuum state is generated through the parametric amplification in a sub-threshold optical parametric oscillator (OPO). A pump of 397 nm and a non-linear PPKTP crystal produce degenerate parametric amplification at the atomic resonance frequency of 795nm. The vertically-polarized squeezed vacuum is combined with a strong, horizontally-polarized coherent beam on a polarization beam splitter (PBS). The relative phase between these two contributions is controlled by a piezo-electric actuator and active feedback using the noise level of the signal as the system variable [36, 66]. The resulting optical beam is horizontally polarized with squeezed fluctuations in the diagonal basis, i.e., squeezed in S_y.

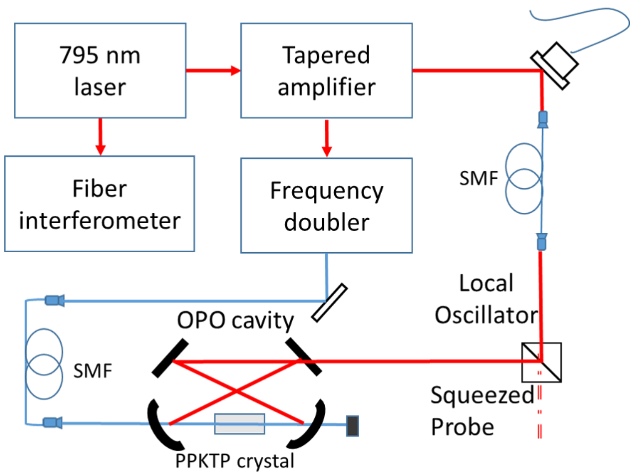

Figure 16: Schematic of the Squeezer OPO setup.

The squeezing is detected with a balanced detection setup that consists of a half wave plate (HWP) at 22.5° followed by a Wollaston prism that splits the beam in the horizontal and vertical components. The two components are detected and electronically subtracted by a commercial switchable gain balanced detector which is photon noise limited at the operational conditions. The signal can be monitored on Spectrum analyser and recorded with a data acquisition card at 200 kSamples/s. Quantum noise locking is used to stabilize the phase of the local oscillator at the level of squeezing or anti-squeezing. A similar balanced detector system is used before the magnetometer to characterize the generated squeezing and allows the comparison with the one detected after the light absorption due to the atomic interaction.

4.1.6 Bell Bloom magnetometer probed with squeezed light

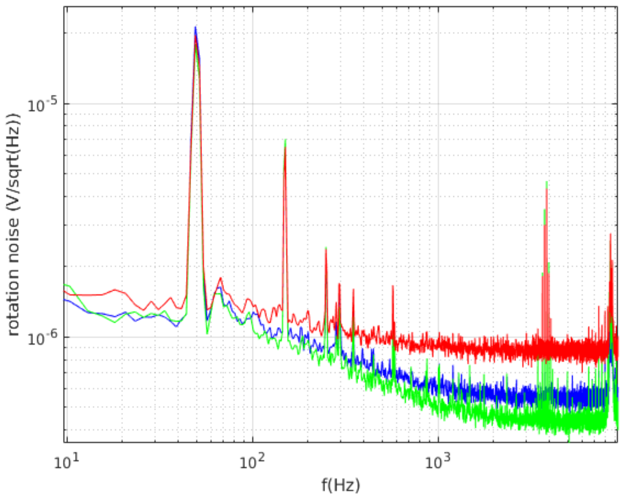

Figure 17: Polarization rotation noise spectrum after the lock-in demodulation of the signal from the Bell Bloom magnetometer operating with 1.5 x 10^{13}atoms/cm^3 precessing at 29 kHz and probed with coherent (blue) and polarization squeezed light (green) and polarization anti-squeezed light (red).

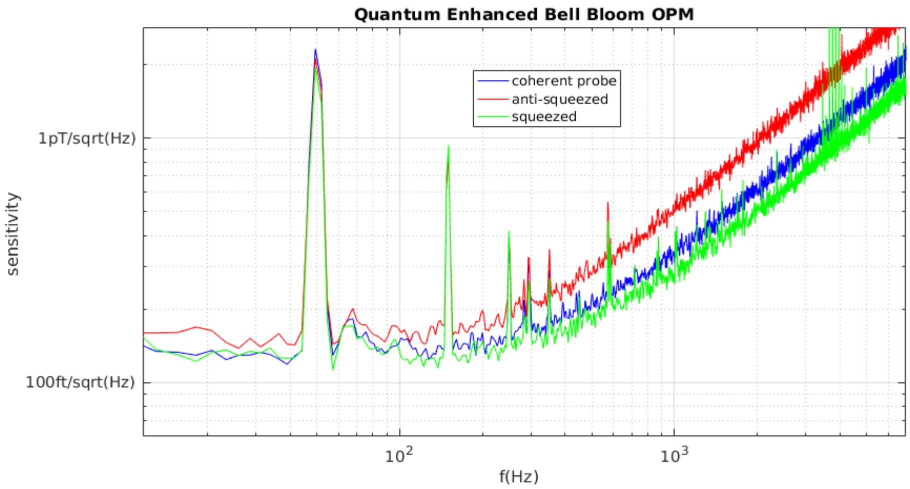

Figure 18: Magnetometer sensitivity as a function of detection frequency for coherent and squeezed light probing. Bias field 4 μT, modulation frequency 29 kHz, Pump power 50 μW, Probe Power 440 μW.

The performance of the magnetometer with and without squeezed light enhancement can be seen in Figure 17 and Figure 18. These show the directly-measured noise spectra of the polarization rotation signal and the inferred magnetic noise sensitivity, respectively. The squeezing reduces the noise level in the PSN-limited regime. Also, by lowering the white-noise background due to photon shot noise, the width of high-sensitivity, low-frequency region is increased. In this sense, the bandwidth of the device is enhanced by squeezing, even though the responsivity $A(\nu)$ is unchanged. This can be seen in Figure 18.

4.1.7 Prospects for the squeezed-light OPM

The above describes a preliminary successful application of squeezed light to a high-sensitivity OPM, achieving a sensitivity more than a factor of 10 better than the previous record for sensitivity in quantum-enhanced OPM [35]. The system also represents an opportunity to study several poorly-understood questions in quantum enhancement of atomic devices.

As already described in Section 3.1, it is an open question whether an atomic quantum sensor, when optimized for atom number and photon flux, will be amenable to quantum enhancement with optical or atomic squeezing. The squeezed-light OPM provides an excellent opportunity to study this question, as the optical squeezer and magnetometry system can be independently optimized.

Other questions of interest are the relationship between quantum enhancement and bandwidth. As mentioned already, reducing the optical quantum noise has the effect of making visible signals that otherwise would be lost due to the roll-off in the responsivity $A(\nu)$. This is closely related to prior work showing that the possibility to recover signal components beyond the natural bandwidth of a sensor using Kalman filtering techniques [67]. These methods are limited by the optical shot noise and would be enhanced as squeezing reduces this noise source.

4.2 Measurement-induced squeezing in SERF-regime alkali vapors

In the single-pass geometry, the achievable spin-squeezing by QND measurement is limited by the effective on-resonance optical depth [68, 69]. In SERF-regime vapors this number can potentially be very high, due to the large number density. At the same time, little is known about spin squeezing in SERF-regime vapors, which show a complicated spin dynamics in which the many-body coherence time is much longer than the single-atom coherence time, see Section 3.2. There is, moreover, not at present a theory of the statistical behaviour of SERF-regime vapors adequate to describe quantum statistical features such as spin squeezing.

To address these issues, ICFO made an experimental and theoretical study of spin squeezing in the SERF regime, using a vapor of ^{87}Rb and off-resonant Faraday rotation probing. The work is described in detail in [70].

The spin dynamics can be described by the time-dependent Hamiltonian

$$H = \hbar A_{hf} \sum_{i} \boldsymbol{j}^{(i)} \cdot \boldsymbol{i}^{(i)} + \hbar \sum_{ll'n} \theta_n \delta(t - t_n^{(l,l')}) \boldsymbol{j}^{(l)} \cdot \boldsymbol{j}^{(l')} + \hbar \sum_{lm} \psi_m \delta(t - t_m^{(l)}) \boldsymbol{j}^{(l)} \cdot \boldsymbol{d}_m^{(l)} + \hbar \gamma_e \sum_{l} \boldsymbol{j}^{(l)} \cdot \boldsymbol{B} \qquad \text{Eq. 18}$$

where the terms describe the hyperfine (HF) interaction, SE collisions, spin-destruction (SD) collisions and Zeeman interaction, respectively. A_{hf} is the HF splitting and $t_n^{(l,l')}$ is the (random) time of the n-th SE collision between atoms l and l', which causes mutual precession of $\boldsymbol{j}^{(l)}$ and $\boldsymbol{j}^{(l')}$ by the (random) angle θ_n. We indicate with R_{SE} the rate at which such collisions move angular momentum between atoms. Similarly, the third term describes rotations about the random direction $\boldsymbol{d}_m^{(l)}$ by random angle ψ_m, and causes spin depolarization at a rate R_{SD}. In the SERF regime, where $A_{hf} \gg R_{SE} \gg \gamma_2 |B|$, the combinded action of the HF and SE terms rapidly thermalizes the spin state, which is to say it generates the maximum entropy state consistent with the ensemble total angular momentum $\boldsymbol{F}$, which is conserved by the SE and HF interactions. We write the thermal state as $\rho_{\boldsymbol{F}}^{(th)}$. On longer time scales, $\boldsymbol{F}$ experiences precession about the magnetic field and relaxation due to SD collisions. The relaxation is necessarily accompanied by fluctuations which can be understood using the fluctuation-dissipation theorem [67].

Already here we see something interesting about SERF regime vapors: although $\rho_{\boldsymbol{F}}^{(th)}$ is thermalized, it can also be a squeezed and entangled state. For example, if $\boldsymbol{F} = \boldsymbol{0}$, then $\rho_{\boldsymbol{F}}^{(th)}$ describes a macroscopic singlet state [71-73] with zero spin noise, far below the quantum noise of any non-entangled state. This remains a high-entropy state, because there are many ways to organize the atomic spins into singlets, and all of these are given equal statistical weight in $\rho_{\boldsymbol{F}}^{(th)}$. More generally, the total spin $\boldsymbol{F}$ will be described by a statistical distribution. The generalized theory of spin squeezing [11, 74] can be used to identify squeezed states based on this distribution. In particular, if the total variance $|\Delta\boldsymbol{F}|^2 \equiv \langle \Delta F_x^2 \rangle + \langle \Delta F_y^2 \rangle + \langle \Delta F_z^2 \rangle$ is sufficiently small, below the standard quantum limit in the sense that it implies atomic entanglement, the state must contain a computable fraction of the atoms in singlet states.

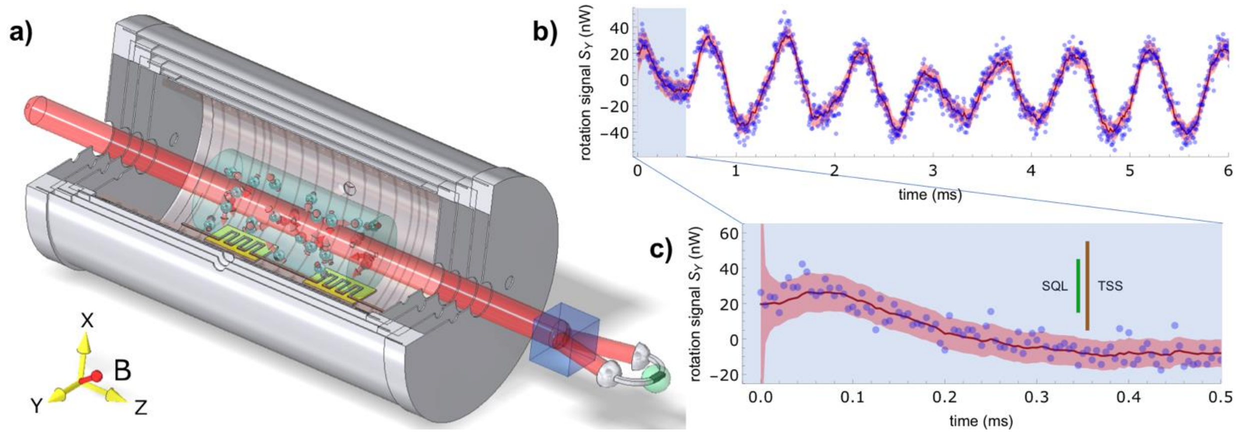

Figure 19: Setup and signals for spin-squeezing by quantum non-demolition measurement in a high-density SERF-regime vapor. Figure from [70]. A) schematic of the experimental setup showing vapor cell, shielding, probe beam and polarization optics for Faraday rotation measurement. B) a short section of recorded signal, showing polarimeter samples (blue dots) and Kalman filter reconstruction, including best estimate (red line) and $\pm 1\sigma$ confidence interval (red shaded region). C) zoom of the earliest part of the time series, showing the rapid reduction of uncertainty leading to uncertainty below the standard quantum limit.

To explore this further, ICFO performed an experiment, illustrated in Figure 19. This employed a vapor of ^{87}Rb with 100 Torr of N_2 buffer gas, and probed with a laser detuned 44 GHz from the D_1 line. A Magnetic field along the 1,1,1 direction produced spin precession, but no optical pumping was applied. A Kalman filter [75] was used to infer the spin state $\boldsymbol{F}$ from the measured data. As shown in Figure 19c, the resulting uncertainty on the spin state rapidly drops below the SQL, confirming that the SERF-regime medium can support squeezing and entanglement.

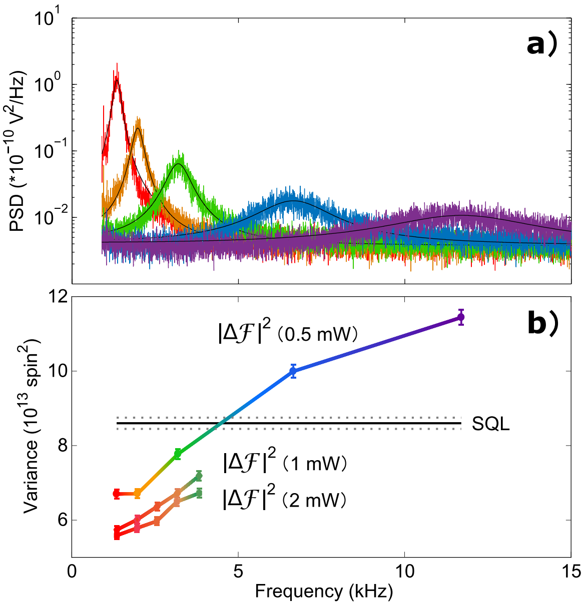

Figure 20: SERF effect suppression of spin relaxation and effect on squeezing. A) shows spin noise spectra for field strengths that produce Larmor frequencies of 1-12 kHz. As the Larmor frequency is reduced below the spin-exchange rate, the resonance linewidth narrows and the signal to noise ration increases dramatically. B) total variance $|\Delta \boldsymbol{F}|^2$ of the signal as a function of Larmor frequency, showing a transition to spin squeezing as the system enters the SERF regime.

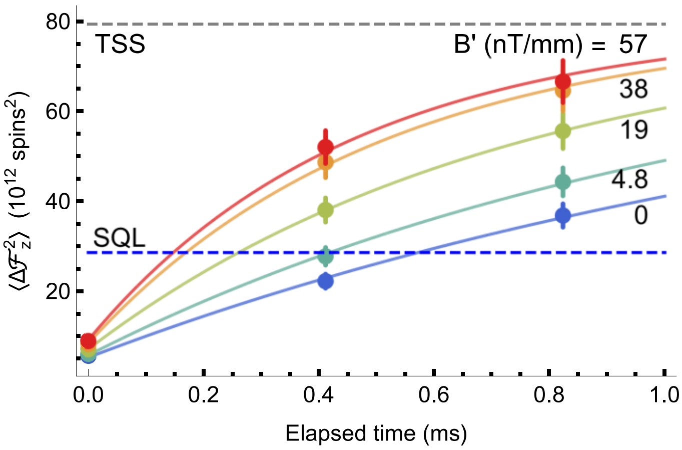

Figure 21: Duration of the squeezing and effect of an applied magnetic field gradient. Again using the Kalman filter, the uncertainty was observed to grow toward a thermal spin state on a few-ms time-scale in the absence of further measurement data input (blue curve). It is notable that the time between SE collisions, the slowest part of the thermalization mechanism, is about 20 µs, meaning the squeezing persists for tens of thermalization times. The effect of a gradient is to accelerate the relaxation toward a thermal state. This provides a measure of the distribution of distances separating the atoms participating in the singlet states, as these singlets convert into noisier triplet states. The inferred typical inter-atomic distance is about 1 mm, whereas the typical nearest-neighbour distance is about 0.1 um.

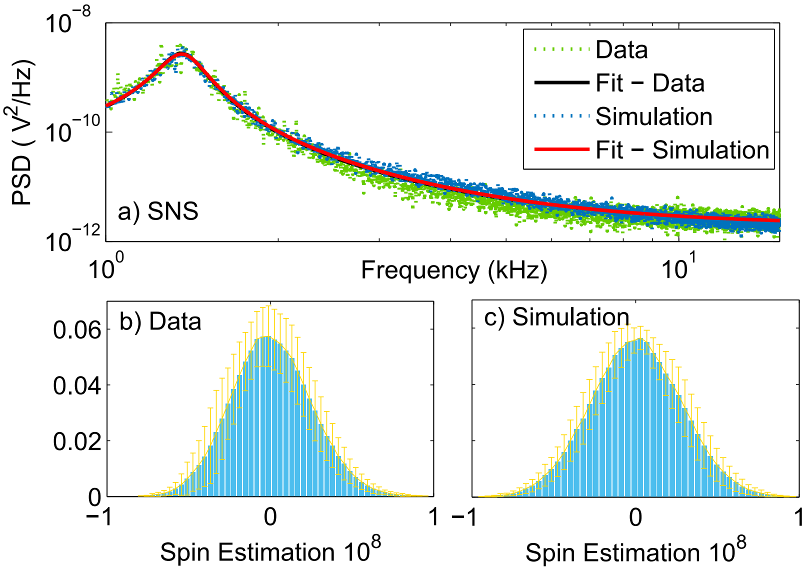

Figure 22 Kalman model validation based on experimental data (Data) and simulated data (Simulation). A) spin noise spectroscopy (SNS) of Data (blue dots) and Simulation (green dots). The Lorentz fittings of Data (black line) and Simulation (red line) are fully overlapped. The spin distributions from Data b) and Simulation c) are shown as histograms. Error bars indicate plus/minus one standard deviation of histograms of 20 traces. Probe power = 2 mW, ν_L = 1.3 kHz.

Additional results from this experiment are shown in Figure 20, Figure 21 and Figure 22. These show that the SERF-regime is in fact favourable to the generation of squeezing in the experiment, that the entanglement and squeezing last for tens of thermalization times and involve atoms separated by thousands of times the nearest-neighbour distance, and show a remarkable agreement between the statistics of the Kalman filter model and the observed results from the experiment.

4.3 Sub-millimetre active volume OPM

4.3.1 Overview and goals

The realization of a sub-mm active volume OPMs has both applied and fundamental interest. Reducing the volume of high-sensitivity atomic sensors is a technological challenge for numerous applications in space science and navigation as well as in bio-medical diagnostics. A comprehensive review on chip-scale atomic sensors has been recently reported in [76], describing how most solutions still make use of mm-size active volumes, combined in more compact devices through anodic bonding with silicon wafers or integrated on the top of photonic waveguides to interact with their evanescent field. Further size reduction and flexibility can significantly improve the spatial resolution of high-sensitivity OPMs in applications like MEG and MCG as well as in the study of materials/solid-state magnetic fields, competing with NV-centers based sensors. On the other hand, atomic sensors with sub-mm active volumes will show higher atomic quantum noise (ASN), which is expected to be the dominant noise contribution over technical noise sources. To keep the sensitivity high, multi-pass [77] or cavity geometries [78] would be necessary to enhance the optical depth of atomic vapours enclosed in microcells. The combination of sub-mm active volume with cavity-enhanced optical depth will make this device a unique platform to study spin squeezing and QND measurements for quantum-enhanced miniaturized OPMs.

4.3.2 Transit time and buffer gas pressure

Sub-mm atomic cells have been also proposed for realization of SI units, like time, on a chip. As shown in Figure 23 (taken from [79]), in small dimensions cells and photonic structures the transit time broadening of atoms across the laser beam increases drastically in absence of buffer gas. For applications where alkali Doppler-free features need to be resolved, like atomic spectroscopy and atomic clocks, a beam size between 10 μm and 1 mm is then favourable. However, evanescent field interrogation can be appropriate for combining photonic structures with sensing of Doppler-broadened transitions. A hybrid approach that expands the photonic waveguide mode to 50 μm for atomic interaction in a mm active volume cell has been recently used for 780 nm laser frequency stabilization with a stability of 10^{-11} [80].

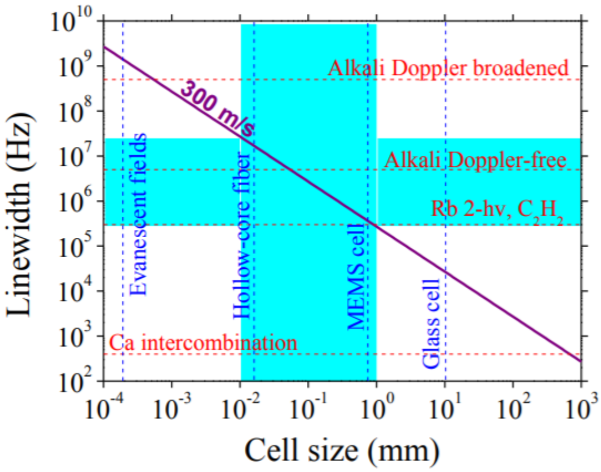

Figure 23: Transit time broadening at room temperature for vapour moving at 300 m/s. Figure from [58].

In OPMs, as well as in other atomic sensors, the transit time broadening is significantly reduced with the addition of inert buffer gas. This is also beneficial, by collisional mixing of excited states, for generation of high atomic polarization, optically-induced by depopulation pumping [81]. For sub-mm active volume, the buffer gas pressure needs to be optimized, similarly to MEMS cells, to balance the relaxation from the inner walls, inversely proportional to the N_2 pressure, and relaxation due to collisions between rubidium and buffer gas, proportional to its pressure.

The sensitivity of OPMs is indeed proportional to the total relaxation linewidth including spin-exchange and spin-destruction rates between Rb atoms:

$$\Gamma_{rel} = R_{WD} + R_{BG} + R_{SE} + R_{SD} \quad \text{Eq. 19}$$

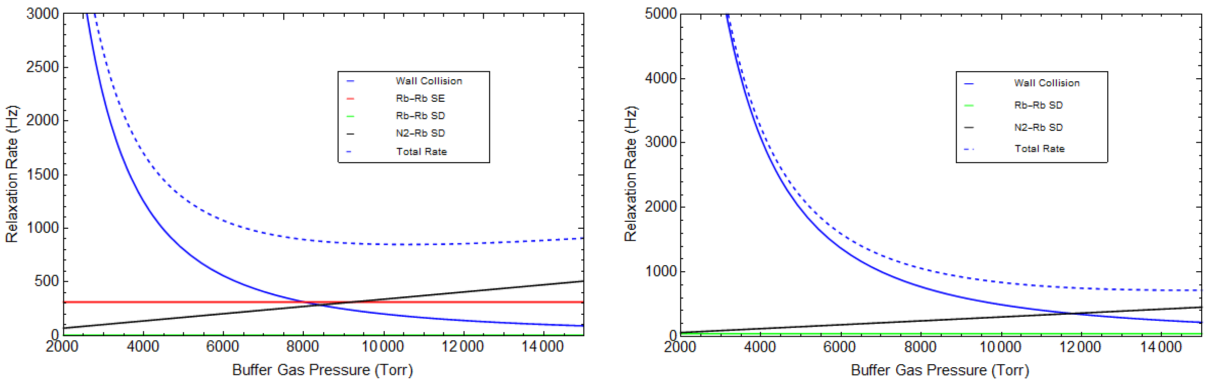

Figure 24: Optimal buffer gas pressure for sub-mm active volume OPM at temperatures T=90°C including spin-exchange collisions (left) and T=190°C without collisions in the SERF regime (right).

Where R_{BG}, R_{SE} and R_{SD} are the relaxation rates due to buffer gas, SE collisions and SD collisions, respectively. The wall relaxation rate is particularly relevant in sub-mm active volume and is given by [82]:

$$R_{WD} = [\left(\frac{\pi}{L}\right)^2 + \left(\frac{2.405}{r}\right)^2]D_0 \,\frac{760}{\varrho_{N_2}}\sqrt{\frac{T}{273.15}\frac{(273.15+T)}{273.15}} \qquad \text{Eq. 20}$$

where ϱ_{N_2} is the nitrogen pressure in Torr, D_0 is the diffusion constant between rubidium and nitrogen, L and r are the cell length and beam waist (radius), respectively. In Figure 24 we show the different contributions and the total relaxation rate for an interaction length L=100 μm and a beam waist of r= 100 μm. We consider a temperature of T=90°C (left), including spin-exchange collisions, and T=190°C (right) in the SERF regime. These theoretical estimations give optimal relaxation rates, in units of linear frequency, of 847.851 Hz and 715.85 with buffer gas pressures of 13.9 atm (10.6 kTorr) and 19.5 atm (14.8 kTorr), respectively. Here we are not limiting the strategy to the SERF operation mode, since total field gradiometers (OPG) based on the subtraction of FID signals from two atomic interaction regions can give comparable sensitivity in detecting biological signals with the great advantage of working in unshielded environment [83]. Furthermore, as previously described in section 2.4.2, FID signals are suitable for continuous QND and BAE measurements when atomic spins freely precess in the transverse plane, along the probe propagation direction.

4.3.3 Projection-noise-limited sensitivity

For N spin-1/2 atoms with coherence time $T_2 = 1/\Gamma_{rel}$, the fundamental sensitivity is limited by the ASN and, after a time of measurement much longer than coherence time $t \gg T_2$ is given by [77, 84]:

$$\delta B = \frac{1}{\gamma}\sqrt{\frac{2\,\exp[1]}{NT_2 t}} \qquad \text{Eq. 21}$$

where $2\pi/\gamma$ is the gyromagnetic ratio in units of T/Hz. Since the total number of atoms N = nV is linear in each number density n and volume V, we can define the fundamental magnetic sensitivity per unit of volume in units of $\mathrm{Tcm}^{3/2}/\sqrt{\mathrm{Hz}}$:

$$\delta B_n = \frac{10^3}{\gamma}\sqrt{\frac{2\,\exp[1]\,\Gamma_{rel}}{nt}}. \qquad \text{Eq. 22}$$

With the optimal relaxation rate of $\Gamma_{rel} = (2\pi)$ x 847.851 Hz, obtained in the previous section at T=90°C, in the presence of high buffer gas pressure and spin-exchange collisions, by using Eq. 22 we calculate that a sensor with sub-mm active volume of V= $\pi r^2 L = \pi\ (100\ \mu m)^3$ would have a fundamental sensitivity of 0.8 $\mathrm{pT}/\sqrt{\mathrm{Hz}}$ and a volume-adjusted sensitivity of 1.4 $\mathrm{fTcm}^{3/2}/\sqrt{\mathrm{Hz}}$. This would improve to sub-$\mathrm{fTcm}^{3/2}/\sqrt{\mathrm{Hz}}$ by increasing the atomic density as shown in Fig. 25, where we report Eq. 22 as function of temperature in °C. This optimal volume-adjusted sensitivity is comparable with state-of-the-art (SOA) sensitivity per unit of volume, obtained in a sub-femtotesla scalar magnetometer with two multi-pass cells with volume of 0.3 cm^3 each. Then, while the absolute sensitivity may limit the magnitude of magnetic field that could be detected, a sub-mm active volume OPM could have a fundamental ASN in the pico-tesla regime, which is attractive for quantum enhancement by QND and BAE measurements.

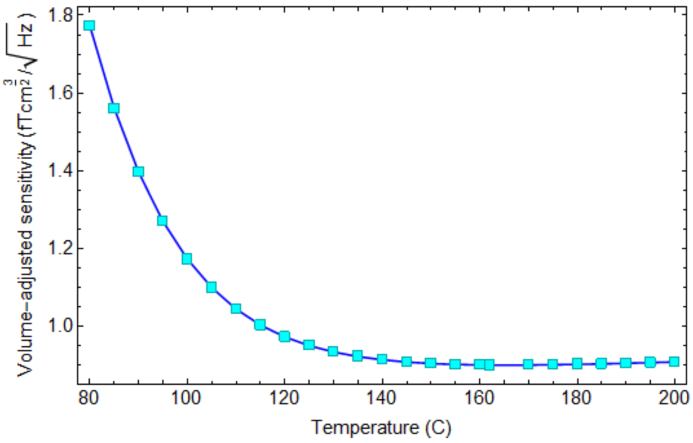

Figure 25: Optimal volume-adjusted projection-noise-limited sensitivity for a sub-mm active volume $V = \pi\ (100\ \mu m)^3$ *versus temperature.*

4.3.4 Multi-pass and cavity-enhanced OPM

Several recent, sensitive scalar OPMs use multi-pass geometries to increase the interaction length by 2 orders of magnitude, reaching sub-fT sensitivity [77], quantum-noise-limited operation in Earth's field [85] and applications in MEG and MCG in unshielded environment [83]. These SOA sensors are based on enhancement of dispersive Faraday rotation thanks to the increased optical depth for an off-resonant probe. The fabrication process consists of active alignment and anodic bonding between mirrors and Pyrex glass with mm to cm active volume. These hybrid cells are fitted with a filling tube, through which they are evacuated and filled with Rb and N_2 with conventional glassblowing techniques. The filling tube, i.e. the cell stem, is finally sealed by heating. In configurations with cylindrical or spherical mirrors [77, 86], the probe beam is focused into a 100 μm hole thorugh one mirror, then it expands within the interaction area and exit after multiple reflections, through the same hole. In geometries with planar mirrors [83], these are cut and relatively shifted to allow a beam with near-zero input angle to undergo multiple reflections and leave the cell. Multi-pass geometries have several advantages like deterministic number of passes and optical length, high input/output power ratio and the possibility of combining an interaction region where the beams expand and overlap with a different one where they are well-separated, in contrast to typical standing wave cavities. The latter feature has been recently used in a direct gradiometer with a single multi-pass cell and allows the atoms to interact with a wide beam region excluding strongly focused areas, that would induce decoherence due to atomic diffusion [77, 87], limiting the possibility of quantum enhancement by spin squeezing.

The fabrication techniques of multi-pass cells become increasingly difficult when the active volume is reduced down to sub-mm dimensions. The implementation of technologically available micro-optics and micro-cavities is an attractive and promising solution. To date, cavity-enhanced atomic sensing techniques have been applied to non-magnetic transitions in atomic systems [45], of interest for atomic clocks, and in an amplitude-modulated nonlinear optical rotation (AMOR) magnetometer [78]. The latter is an absorptive measurement where, due to optically-induced atomic alignment, in the presence of a magnetic field the atomic medium works like a rotating polarizer causing a rotation in a linearly polarized probe. Here we propose to cavity-enhance a dispersive Faraday rotation in the presence of high degree of atomic orientation, similarly to SOA multi-pass sensors, but considering a sub-mm active volume OPM.

4.3.5 Faraday rotation in transmission

We start considering a bi-concave cavity with length L that consists of two cavity mirrors M_1, M_2 with reflectance R_1 (R_2) and transmittance T_1 (T_2), respectively. The input probe field E_{in} is linearly polarized, which is a linear combination of σ^+ and σ^- circular polarizations, while E_T (E_R) is the transmitted (reflected) electric field. The probe beam waist is w_0 and we consider two additional glass surfaces with transmittance T_G that enclose the atomic vapour. We also assume that optically pumping with a second laser (not shown) has previously generated high atomic polarization $P_x = 2\langle S_x \rangle$, where $\langle S_x \rangle$ is the averaged electron spin component along the probe direction, transverse with respect to the applied magnetic field $\vec{B}$, so that the atomic ensemble freely precess in the transverse plane.

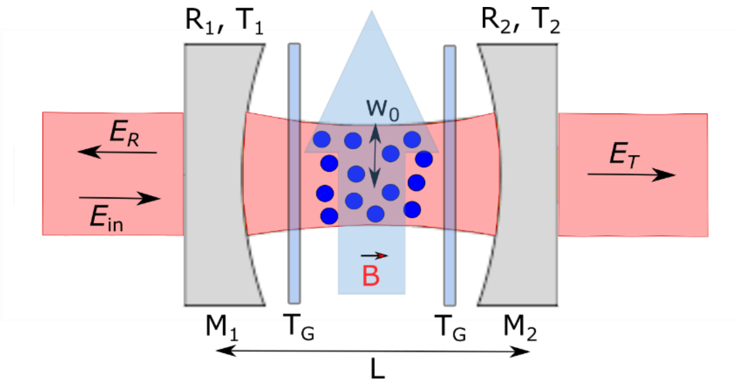

Figure 26: Sketch of sub-mm active volume OPM in a bi-concave cavity for enhancement of dispersive paramagnetic Faraday rotation in transmission.

For a far-detuned probe with detuning Δ from atomic resonance, the paramagnetic Faraday rotation can be written as [77, 81] $\phi(t) = \phi_0 \sin(2\pi\upsilon_L t)\exp[-t/T_2]$, where T_2 is the transverse relaxation rate, υ_L is the Larmor frequency and the initial/maximum rotation is given by:

$$\phi_0 = \frac{n r_e f_{osc}}{2\Delta} G(\mathcal{F}) L P_x \qquad \text{Eq. 23}$$

where n is the atomic number density, r_e is the electron radius and f_{osc} is the oscillation strength of the rubidium D_2 line. Here we introduce $G(\mathcal{F}) > 1$ as the gain in Faraday rotation due to a cavity with finesse $\mathcal{F}$, in contrast with the single-pass scenario where $G(\mathcal{F}) = 1$. For a purely dispersive, non-absorbing media, cavity enhancement of the Faraday effect has been predicted to be proportional to the cavity finesse [88]. For resonantly absorbing media, as in nonlinear Faraday rotation [78], higher intra-cavity power may lead to further intra-cavity losses and power broadening of the atomic transitions involved [89]. Here we consider the purely dispersive case with finesse and rotation gain given by [88]:

$$\mathcal{F} = \frac{\pi\sqrt{R_1R_2}}{1-\sqrt{R_1R_2}} \quad \text{and} \quad G(\mathcal{F}) = \frac{\sqrt{(1+R_1)(1+R_2)}}{\sqrt{(1-R_1)(1-R_2)}} \qquad \text{Eq. 24}$$

In a typical balanced polarimetry detection, the detected signal, i.e. the $\langle S_y \rangle$ Stokes polarization parameter, is proportional to the rotation angle. Then, in the scheme of Figure 25, we can calculate the improvement in signal to noise ratio between single pass and cavity-enhanced conditions. We can use the Jones matrix approach starting with the input vector $E_{in} \equiv \left(E_{in}^{(+)}, E_{in}^{(-)}\right)^T$, where $E_{in}^{(\pm)}$ are the electric field amplitudes for the $\sigma^{\pm}$ circular components, respectively, to get reflected and transmitted electric field. With fixed R_1=0.99 we calculate the SNR enhancement and the ratio of transmitted power between single pass and on-resonance cavity enhancement, versus the second cavity mirror reflectance R_2, as shown in Figure 27. This optimal value decreases when transmission losses through the two surfaces of the vapour cell are included (T_G < 1) causing a reduction in both cavity finesse and rotation gain.

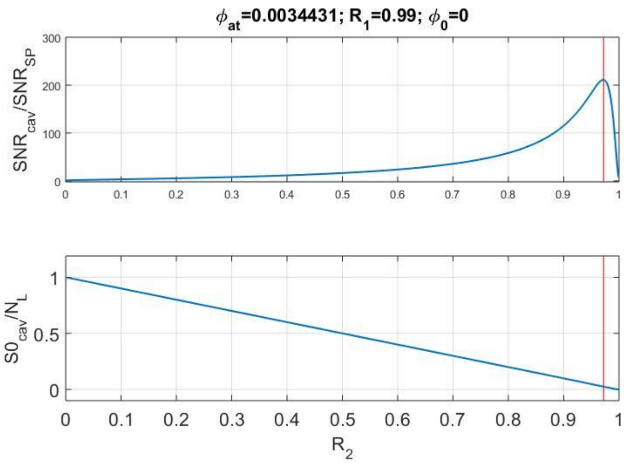

Figure 27: SNR ratio between cavity-enhanced and single pass conditions (top) and percentage of transmitted power (bottom) versus reflectance R_2 of the second cavity mirror.

In Table 1, we report the optimal reflectance R_2 for maximum SNR enhancement and the calculated finesse and rotation gain from Eq. 24 for different transmission losses.

Table 1. SNR ratio between on-resonance cavity-enhanced and single pass conditions (top) and percentage of transmitted power (bottom) versus reflectance R_2 of the second cavity mirror.

T_g	SNR enhancement	R2 (max SNR enhancement)	Finesse	Rotation Gain	Transmitted Power ratio
1	200	97.2 %	161.8	92	2.5%
0.9998	199.8	97.1 %	157.6	87.5	2.6%
0.9996	189.3	97.1 %	157	84.8	2.63
0.985	28.5	88.8 %	47.21	15.6	10%

As example, the single pass maximum rotation for a sub-mm active volume with interaction length L= 100 μm, temperature of T=100°C and buffer gas pressure of 100 Torr would be $\phi_0^{SP} \cong 3$ mrad while the cavity would enhance it by a factor 92 in absence of transmission losses, T_G = 1, to $\phi_0^{cav} \cong 0.3$ rad. We report these simulated signals in Figure 28, with a relaxation time of about $T_2 \cong 2$ ms at different timescale. As discussed in section 4.3.2, the optimal buffer gas pressure should be significantly higher, to avoid depolarization by collisions with the inner walls. For 10^4 Torr, we calculate a reduced maximum rotation of $\phi_0^{SP} \cong 0.7$ mrad and $\phi_0^{cav} \cong 60$ mrad. The need for cavity or multipass enhancement in sub-mm active volume OPM is now clearer, because the short interaction length and the high buffer gas pressure significantly limit the achievable maximum rotation in single pass configuration. We also stress that the FID strategy is suitable for continuous generation of spin squeezing with QND and BAE measurements, as previously discussed in section 2.4.2.

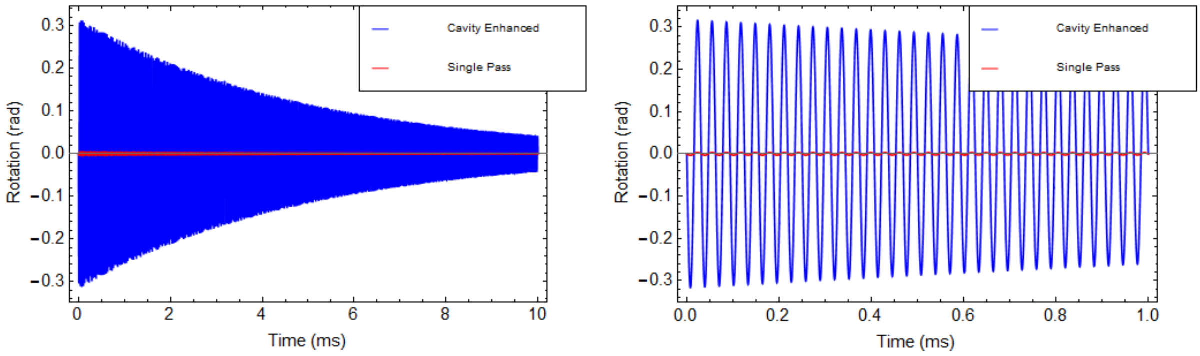

Figure 28: FID signal for single pass and cavity-enhanced Faraday rotation in transmission.

So far, we have not made any assumption on cavity mirror curvatures and beam waist. This is important by considering the current available technology in curvature machining of fibres and fused silica glass for high-finesse micro-cavities [90]. In OPMs with thermal vapours, atoms diffuse across the interaction area such that a uniform beam radius is favourable with respect to strongly focused beams, as in SOA high-finesse cavities, to prevent decoherence of quantum correlations by diffusion [77, 87]. In sub-mm active volume with L= 100 μm it would be good to have a pseudo-collimated beam, on resonance with the cavity. This condition is satisfied for w_0 = 100 μm but it requires machining of long radius of curvature on cavity mirrors/surfaces. In Table 2 we calculate the radius of curvature at distance L/2=50 μm for a Gaussian beam with waist w_0 = 25, 50 and 100 μm, respectively. For w_0 = 100 μm the cavity mirrors curvature is on the order of tens of meters, while it's reduced to hundreds of mm for a 1 cm long cavity.

Table 2: Radius of curvature for a Gaussian beam at distance z=50 μm, 2.5 mm and 5 mm for different beam waists. Note: these calculations are performed in free space with no atoms.

Beam waist at z=0	Radius at z=50 μm	d/R	Radius at z=2.5 mm	d/R	Radius at z = 5 mm	d/R
25 micron	122 mm	8.19e-4	4.9 mm	1.02	6.2 mm	1.62
50 micron	1.95 m	5.12e-5	41.5 mm	0.12	24.5 mm	0.4
100 micron	31 m	6.45e-5	627 mm	0.007	317 mm	0.03

Because of this non-trivial technical challenge in curvature machining, we also consider a planar cavity, which could be a simpler solution for a low-finesse regime of operation. In Figure 29, we depict a different configuration, with four surfaces where high-reflectivity coating is applied on the outer surfaces with reflectance R_1 and R_4, respectively. The transmitted over input electric field ratio is shown in the right figure as function of the intermediate distance L2 ≅100 μm for a sub-mm active volume.

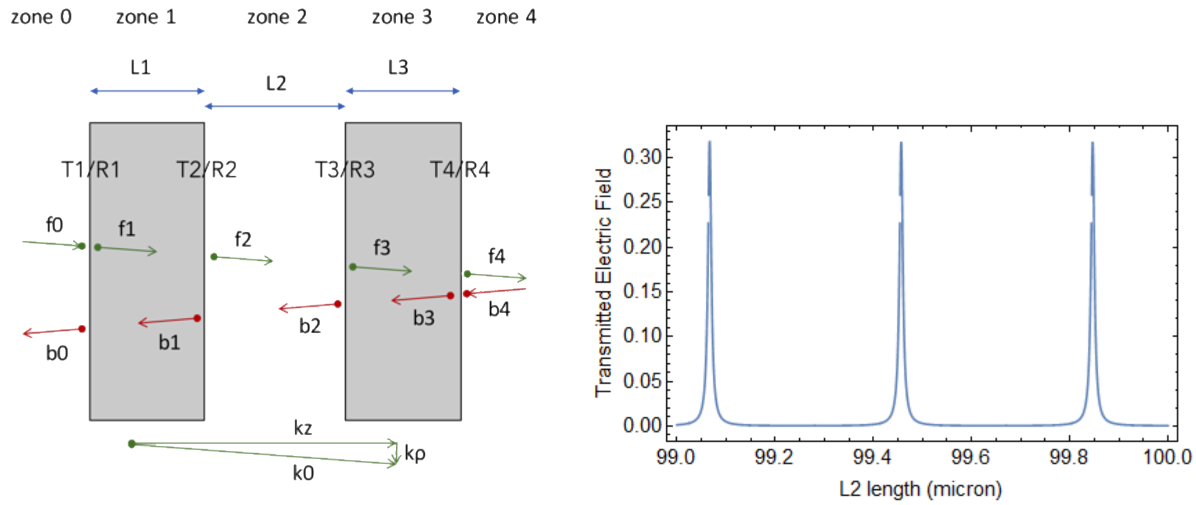

Figure 29: (Left) Planar Fabry-Perot cavity with high-reflectivity coated surfaces with reflectance R_1 and R_4. (Right) Percentage of transmission of input electric field in a four surfaces problem with T1=$\sqrt{0.1}$, T2=T3= T1=$\sqrt{0.96}$ and T4=$\sqrt{0.01}$, where $R_i = \sqrt{1 - T_i^{\,2}}$.

For a beam waist of w_0 = 100 μm we can calculate the reflected radial power density in the on-resonance and off-resonance condition. In Figure 31, the power density profile is reported as function of the radial distance from the propagation axis. Since over the short distance L2 the probe beam with 100 μm waist is pseudo-collimated, the intensity distribution on-resonance remains in the main Gaussian after propagation through the four surfaces. Furthermore, the reflected beam off-resonance is exactly the same since most of light is just reflected back, as shown in the right of Figure 31.

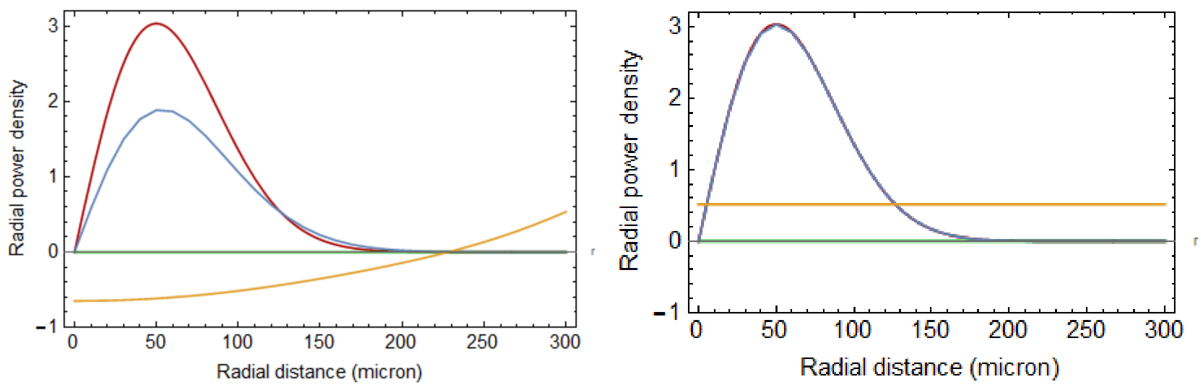

Figure 30: On resonance radial power density of reflected beam (blue) and input beam (red) with phase argument in yellow and green, respectively. (Right) Off-resonance condition.

4.3.6 Cavity enhancement in reflection

While cavity-enhancement of Faraday rotation in transmission is promising for experimental realization, there are some non-trivial aspects like degeneracy of cavity resonance for different linear polarization and interference with the reflected beam that justify the study of different approaches. Here we propose a solution based on Pound-Drever-Hall (PDH) laser locking to a cavity in reflection [91] with the same cavity surfaces and transmittances shown in Figure 29. In Figure 31 we show the proposed setup. A 795 nm pulsed laser induces atomic polarization, not much affected by the cavity due to the strong on-resonance absorption, and weak reflectivity of the cavity mirrors at this wavelength. A circularly polarized 780 nm probe is used for Pound-Drever-Hall (PDH) measurement and stabilization of the laser frequency relative to the cavity resonance. A representative signal is shown in the right panel of Figure 31. The PDH locking technique is a well-established metrology strategy to lock the laser frequency to a cavity resonance, by generating an asymmetric error signal, with respect to the cavity condition [91].

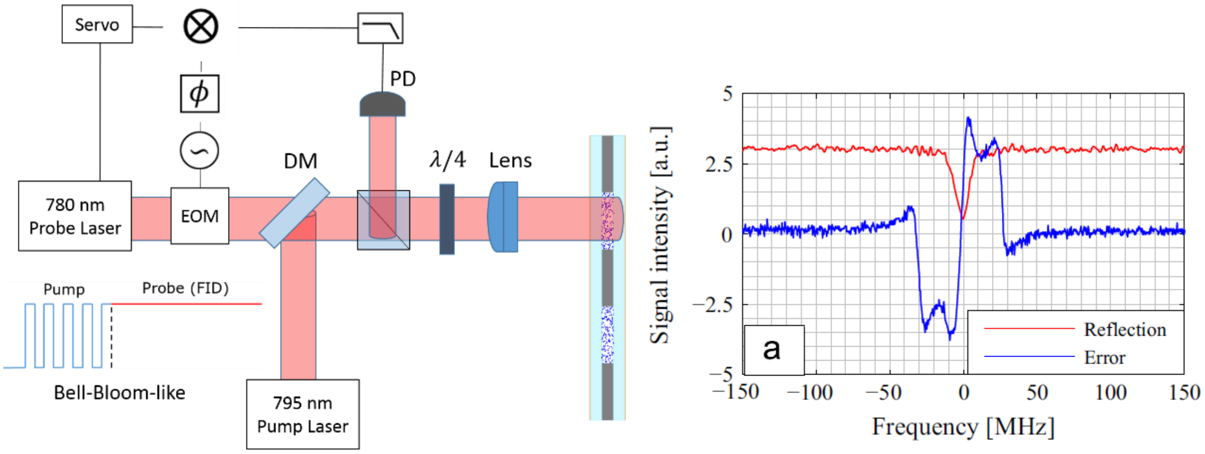

Figure 31: (Left) Cavity-enhancement of atomic interaction by PDH detection in reflection. (Right) Reflected intensity and PDH error signal for laser frequency locking to resonance (from [91]).

The circularly polarized probe undergoes a polarization-dependent phase shift due to atomic interaction. This phase shift is nothing else that the index of refraction of the atomic medium for σ± circular polarization that, for the rubidium D_2 line, is [81]:

$$n^{+}(\nu) = 1 + (1 + P_x/2)\left(\frac{n r_e c^2 f_{D2}}{4\nu}\right)\mathcal{D}(\nu - \nu_{D2}) \quad \text{Eq. 25}$$

$$n^{-}(\nu) = 1 + (1 - P_x/2)\left(\frac{n r_e c^2 f_{D2}}{4\nu}\right)\mathcal{D}(\nu - \nu_{D2}) \quad \text{Eq. 26}$$

where $\mathcal{D}(\nu - \nu_{D2}) = (\nu - \nu_{D2})/((\nu - \nu_{D2})^2 + \left(\frac{\Delta\nu}{2}\right)^2)$ is the dispersion profile around the Rb D_2 line with buffer gas broadened linewidth Δν. Again, we see the dependence on the optically-induced atomic polarization P_x. For a linearly polarized probe, the difference between Eq. 25 and Eq. 26 gives rise to the Faraday rotation of Eq. 23. For a linearly polarized probe, the difference between Eq. 25 and Eq. 26 gives rise to the Faraday rotation of Eq. 23.

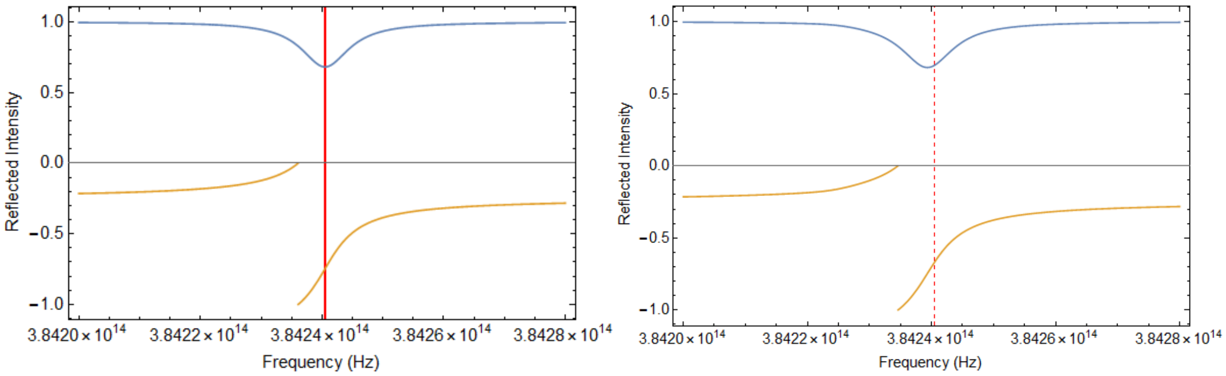

Figure 32: (Left) Reflected intensity and phase versus laser frequency with no atoms. (Right) Reflected intensity and phase versus laser frequency with atoms and intermediate length shift $L_2 \rightarrow n^{+}L_2$.

A circularly polarized probe σ⁺ undergoes a phase shift $E^{(+)} = E_0 \exp[-ikn^{+}L_2]$ while, at the same time, the cavity resonance length changes from resonance condition $L_2 \rightarrow n^{+}L_2$. In Figure 32 we show the change of resonance condition induced by the atomic medium refractive index on a circularly polarized probe. We are currently investigating the dependence of this feature on magnetic field in order to define the advantages of cavity enhancement in the described strategy with detection in reflection.

5 References

[1] V. Braginsky, and Y. Vorontsov, 1974, "Quantum mechanical limitations in macroscopic experiments and modern experimental technique," *Usp Fiz. Nauk* **114**, 41-53.

[2] C. W. Helstrom, 1969, "Quantum detection and estimation theory," *J. Stat. Phys.* **1**, 231-252.

[3] V. B. Braginsky, Y. I. Vorontsov, and K. S. Thorne, 1980, "Quantum Nondemolition Measurements," *Science* **209**, 547-557. http://www.sciencemag.org/content/209/4456/547.abstract

[4] V. Giovannetti, S. Lloyd, and L. Maccone, 2006, "Quantum Metrology," *Physical Review Letters* **96**, 010401. https://link.aps.org/doi/10.1103/PhysRevLett.96.010401

[5] C. M. Caves, 1981, "Quantum-mechanical noise in an interferometer," *Phys. Rev. D* **23**, 1693-1708. http://link.aps.org/doi/10.1103/PhysRevD.23.1693

[6] e. J. Aasi, and et al., 2013, "Enhanced sensitivity of the LIGO gravitational wave detector by using squeezed states of light," *Nat Photon* **7**, 613-619. http://dx.doi.org/10.1038/nphoton.2013.177

[7] T. L. S. Collaboration, 2011, "A gravitational wave observatory operating beyond the quantum shot-noise limit," *Nat Phys* **7**, 962-965. http://dx.doi.org/10.1038/nphys2083

[8] M. Kitagawa, and M. Ueda, 1993, "Squeezed spin states," *Phys. Rev. A* **47**, 5138-5143. http://link.aps.org/doi/10.1103/PhysRevA.47.5138

[9] D. J. Wineland, J. J. Bollinger, W. M. Itano, and D. J. Heinzen, 1994, "Squeezed atomic states and projection noise in spectroscopy," *Phys. Rev. A* **50**, 67-88. http://link.aps.org/doi/10.1103/PhysRevA.50.67

[10] A. Sørensen, L.-M. Duan, J. I. Cirac, and P. Zoller, 2001, "Many-particle entanglement with Bose-Einstein condensates," *Nature* **409**, 63-66.

[11] O. Gühne, and G. Tóth, 2009, "Entanglement detection," *Physics Reports* **474**, 1 - 75. http://www.sciencedirect.com/science/article/pii/S0370157309000623

[12] A. Kuzmich, N. B. Bigelow, and L. Mandel, 1998, "Atomic quantum non-demolition measurements and squeezing," *Europhys. Lett.* **42**, 481-486. http://iopscience.iop.org/0295-5075/42/5/481/?ejredirect=.iopscience

[13] M. H. Schleier-Smith, I. D. Leroux, and V. Vuletić, 2010, "States of an Ensemble of Two-Level Atoms with Reduced Quantum Uncertainty," *Phys. Rev. Lett.* **104**, 073604. https://link.aps.org/doi/10.1103/PhysRevLett.104.073604

[14] G. Colangelo, F. Martin Ciurana, G. Puentes, M. W. Mitchell, and R. J. Sewell, 2017, "Entanglement-Enhanced Phase Estimation without Prior Phase Information," *Phys. Rev. Lett.* **118**, 233603. https://link.aps.org/doi/10.1103/PhysRevLett.118.233603

[15] L. Pezzè, A. Smerzi, M. K. Oberthaler, R. Schmied, and P. Treutlein, 2018, "Quantum metrology with nonclassical states of atomic ensembles," *Reviews of Modern Physics* **90**, 035005. https://link.aps.org/doi/10.1103/RevModPhys.90.035005

[16] V. Giovannetti, S. Lloyd, and L. Maccone, 2004, "Quantum-Enhanced Measurements: Beating the Standard Quantum Limit," *Science* **306**, 1330-1336. http://www.sciencemag.org/content/306/5700/1330.abstract

[17] J. Aasi*, et al.*, 2013, "Enhanced sensitivity of the LIGO gravitational wave detector by using squeezed states of light," *Nat Photon* **7**, 613-619. http://dx.doi.org/10.1038/nphoton.2013.177

[18] C. Virgo*, et al.*, 2019, "Increasing the Astrophysical Reach of the Advanced Virgo Detector via the Application of Squeezed Vacuum States of Light," *Physical Review Letters* **123**, 231108. https://link.aps.org/doi/10.1103/PhysRevLett.123.231108

[19] L.-A. Wu, H. J. Kimble, J. L. Hall, and H. Wu, 1986, "Generation of Squeezed States by Parametric Down Conversion," *Phys. Rev. Lett.* **57**, 2520-2523. http://link.aps.org/doi/10.1103/PhysRevLett.57.2520

[20] H. Vahlbruch, M. Mehmet, K. Danzmann, and R. Schnabel, 2016, "Detection of 15 dB Squeezed States of Light and their Application for the Absolute Calibration of Photoelectric Quantum Efficiency," *Phys. Rev. Lett.* **117**, 110801. http://link.aps.org/doi/10.1103/PhysRevLett.117.110801

[21] G. Hétet, O. Glöckl, K. A. Pilypas, C. C. Harb, B. C. Buchler, H. A. Bachor, and P. K. Lam, 2006, "Squeezed light for bandwidth-limited atom optics experiments at the rubidium D1 line," *Journal of Physics B: Atomic, Molecular and Optical Physics* **40**, 221-226. http://dx.doi.org/10.1088/0953-4075/40/1/020

[22] Y. Han, X. Wen, J. He, B. Yang, Y. Wang, and J. Wang, 2016, "Improvement of vacuum squeezing resonant on the rubidium D1 line at 795 nm," *Optics Express* **24**, 2350-2359. http://www.opticsexpress.org/abstract.cfm?URI=oe-24-3-2350

[23] R. E. Slusher, L. W. Hollberg, B. Yurke, J. C. Mertz, and J. F. Valley, 1985, "Observation of Squeezed States Generated by Four-Wave Mixing in an Optical Cavity," *Phys. Rev. Lett.* **55**, 2409-2412. http://link.aps.org/doi/10.1103/PhysRevLett.55.2409

[24] C. F. McCormick, A. M. Marino, V. Boyer, and P. D. Lett, 2008, "Strong low-frequency quantum correlations from a four-wave-mixing amplifier," *Physical Review A* **78**, 043816. <Go to ISI>://WOS:000260574100156

[25] M.-C. Wu, B. L. Schmittberger, N. R. Brewer, R. W. Speirs, K. M. Jones, and P. D. Lett, 2019, "Twin-beam intensity-difference squeezing below 10 Hz," *Optics Express* **27**, 4769-4780. http://www.opticsexpress.org/abstract.cfm?URI=oe-27-4-4769

[26] N. Corzo, A. M. Marino, K. M. Jones, and P. D. Lett, 2011, "Multi-spatial-mode single-beam quadrature squeezed states of light from four-wave mixing in hot rubidium vapor," *Optics Express* **19**, 21358-21369. http://www.opticsexpress.org/abstract.cfm?URI=oe-19-22-21358

[27] E. E. Mikhailov, and I. Novikova, 2008, "Low-frequency vacuum squeezing via polarization self-rotation in Rb vapor," *Opt. Lett.* **33**, 1213-1215. http://ol.osa.org/abstract.cfm?URI=ol-33-11-1213

[28] J. Ries, B. Brezger, and A. I. Lvovsky, 2003, "Experimental vacuum squeezing in rubidium vapor via self-rotation," *Phys. Rev. A* **68**, 025801. http://link.aps.org/doi/10.1103/PhysRevA.68.025801

[29] A. B. Matsko, I. Novikova, G. R. Welch, D. Budker, D. F. Kimball, and S. M. Rochester, 2002, "Vacuum squeezing in atomic media via self-rotation," *Phys. Rev. A* **66**, 043815. https://link.aps.org/doi/10.1103/PhysRevA.66.043815

[30] S. Ast, M. Mehmet, and R. Schnabel, 2013, "High-bandwidth squeezed light at 1550 nm from a compact monolithic PPKTP cavity," *Opt. Express* **21**, 13572-13579. http://www.opticsexpress.org/abstract.cfm?URI=oe-21-11-13572

[31] J. A. Zielińska, and M. W. Mitchell, 2018, "Atom-resonant squeezed light from a tunable monolithic ppRKTP parametric amplifier," *Opt. Lett.* **43**, 643-646. http://ol.osa.org/abstract.cfm?URI=ol-43-4-643

[32] D. M. Klyshko, 1997, "Polarization of light: Fourth-order effects and polarization-squeezed states," *Journal of Experimental and Theoretical Physics* **84**, 1065-1079. http://dx.doi.org/10.1134/1.558243

[33] N. Korolkova, G. Leuchs, R. Loudon, T. C. Ralph, and C. Silberhorn, 2002, "Polarization squeezing and continuous-variable polarization entanglement," *Phys. Rev. A* **65**, 052306. http://link.aps.org/doi/10.1103/PhysRevA.65.052306

[34] R. Schnabel, W. P. Bowen, N. Treps, T. C. Ralph, H.-A. Bachor, and P. K. Lam, 2003, "Stokes-operator-squeezed continuous-variable polarization states," *Phys. Rev. A* **67**, 012316. http://link.aps.org/doi/10.1103/PhysRevA.67.012316

[35] T. Horrom, R. Singh, J. P. Dowling, and E. E. Mikhailov, 2012, "Quantum-enhanced magnetometer with low-frequency squeezing," *Phys. Rev. A* **86**, 023803. http://link.aps.org/doi/10.1103/PhysRevA.86.023803

[36] F. Wolfgramm, A. Cerè, F. A. Beduini, A. Predojević, M. Koschorreck, and M. W. Mitchell, 2010, "Squeezed-Light Optical Magnetometry," *Phys. Rev. Lett.* **105**, 053601. https://link.aps.org/doi/10.1103/PhysRevLett.105.053601

[37] E. J., G. C., W. A., G. S., and O. M. K., 2008, "Squeezing and entanglement in a Bose-Einstein condensate," *Nature* **455**, 1216-1219. http://www.nature.com/nature/journal/v455/n7217/suppinfo/nature07332_S1.html

[38] M. F. Riedel, P. Böhi, Y. Li, T. W. Hänsch, A. Sinatra, and P. Treutlein, 2010, "Atom-chip-based generation of entanglement for quantum metrology," *Nature* **464**, 1170-1173. http://dx.doi.org/10.1038/nature08988

[39] B. Lücke*, et al.*, 2011, "Twin Matter Waves for Interferometry Beyond the Classical Limit," *Science* **334**, 773. http://science.sciencemag.org/content/334/6057/773.abstract

[40] C. D. Hamley, C. S. Gerving, T. M. Hoang, E. M. Bookjans, and M. S. Chapman, 2012, "Spin-nematic squeezed vacuum in a quantum gas," *Nat Phys* **8**, 305--308. http://dx.doi.org/10.1038/nphys2245

[41] I. D. Leroux, M. H. Schleier-Smith, and V. Vuletić, 2010, "Implementation of Cavity Squeezing of a Collective Atomic Spin," *Phys. Rev. Lett.* **104**, 073602. https://link.aps.org/doi/10.1103/PhysRevLett.104.073602

[42] O. Hosten, R. Krishnakumar, N. J. Engelsen, and M. A. Kasevich, 2016, "Quantum phase magnification," *Science* **352**, 1552. http://science.sciencemag.org/content/352/6293/1552.abstract

[43] W. Muessel, H. Strobel, D. Linnemann, D. B. Hume, and M. K. Oberthaler, 2014, "Scalable Spin Squeezing for Quantum-Enhanced Magnetometry with Bose-Einstein Condensates," *Phys. Rev. Lett.* **113**, 103004. https://link.aps.org/doi/10.1103/PhysRevLett.113.103004

[44] C. F. Ockeloen, R. Schmied, M. F. Riedel, and P. Treutlein, 2013, "Quantum Metrology with a Scanning Probe Atom Interferometer," *Physical Review Letters* **111**, 143001. https://link.aps.org/doi/10.1103/PhysRevLett.111.143001

[45] O. Hosten, N. J. Engelsen, R. Krishnakumar, and M. A. Kasevich, 2016, "Measurement noise 100 times lower than the quantum-projection limit using entangled atoms," *Nature* **529**, 505-508. http://dx.doi.org/10.1038/nature16176

[46] T. Takano, M. Fuyama, R. Namiki, and Y. Takahashi, 2009, "Spin Squeezing of a Cold Atomic Ensemble with the Nuclear Spin of One-Half," *Physical Review Letters* **102**, 033601. https://link.aps.org/doi/10.1103/PhysRevLett.102.033601

[47] J. Appel, P. J. Windpassinger, D. Oblak, U. B. Hoff, N. Kjærgaard, and E. S. Polzik, 2009, "Mesoscopic atomic entanglement for precision measurements beyond the standard quantum limit," *Proc. Nat. Acad. Sci.* **106**, 10960-10965. http://www.pnas.org/content/106/27/10960.abstract

[48] R. J. Sewell, M. Koschorreck, M. Napolitano, B. Dubost, N. Behbood, and M. W. Mitchell, 2012, "Magnetic Sensitivity Beyond the Projection Noise Limit by Spin Squeezing," *Phys. Rev. Lett.* **109**, 253605. http://link.aps.org/doi/10.1103/PhysRevLett.109.253605

[49] J. G. Bohnet, K. C. Cox, M. A. Norcia, J. M. Weiner, Z. Chen, and J. K. Thompson, 2014, "Reduced spin measurement back-action for a phase sensitivity ten times beyond the standard quantum limit," *Nat Photon* **8**, 731-736. http://dx.doi.org/10.1038/nphoton.2014.151

[50] V. Shah, G. Vasilakis, and M. V. Romalis, 2010, "High bandwidth atomic magnetometery with continuous quantum nondemolition measurements," *Phys Rev Lett* **104**, 013601. http://dx.doi.org/10.1103/PhysRevLett.104.013601

[51] G. Vasilakis, V. Shah, and M. V. Romalis, 2011, "Stroboscopic Backaction Evasion in a Dense Alkali-Metal Vapor," *Phys. Rev. Lett.* **106**, 143601. http://link.aps.org/doi/10.1103/PhysRevLett.106.143601

[52] G. Vasilakis, H. Shen, K. Jensen, M. Balabas, D. Salart, B. Chen, and E. S. Polzik, 2015, "Generation of a squeezed state of an oscillator by stroboscopic back-action-evading measurement," *Nature Physics* **11**, 389-392. http://dx.doi.org/10.1038/nphys3280

[53] F. Martin Ciurana, G. Colangelo, L. Slodička, R. J. Sewell, and M. W. Mitchell, 2017, "Entanglement-Enhanced Radio-Frequency Field Detection and Waveform Sensing," *Phys. Rev. Lett.* **119**, 043603. https://link.aps.org/doi/10.1103/PhysRevLett.119.043603

[54] G. Colangelo, F. M. Ciurana, L. C. Bianchet, R. J. Sewell, and M. W. Mitchell, 2017, "Simultaneous tracking of spin angle and amplitude beyond classical limits," *Nature* **543**, 525-528. http://dx.doi.org/10.1038/nature21434

[55] V. G. Lucivero, A. Dimic, J. Kong, R. Jiménez-Martínez, and M. W. Mitchell, 2017, "Sensitivity, quantum limits, and quantum enhancement of noise spectroscopies," *Phys. Rev. A* **95**, 041803. https://link.aps.org/doi/10.1103/PhysRevA.95.041803

[56] V. G. Lucivero, R. Jiménez-Martínez, J. Kong, and M. W. Mitchell, 2016, "Squeezed-light spin noise spectroscopy," *Phys. Rev. A* **93**, 053802. http://link.aps.org/doi/10.1103/PhysRevA.93.053802

[57] S. A. Crooker, D. G. Rickel, A. V. Balatsky, and D. L. Smith, 2004, "Spectroscopy of spontaneous spin noise as a probe of spin dynamics and magnetic resonance," *Nature* **431**, 49-52. https://doi.org/10.1038/nature02804

[58] M.-Z. Huang, *Spin squeezing and spin dynamics in a trapped-atom clock* 2019, (Sorbonne Université). https://tel.archives-ouvertes.fr/tel-02356949

[59] B. Julsgaard, A. Kozhekin, and E. S. Polzik, 2001, "Experimental long-lived entanglement of two macroscopic objects," *Nature* **413**, 400-403. https://doi.org/10.1038/35096524

[60] W. Wasilewski, K. Jensen, H. Krauter, J. J. Renema, M. V. Balabas, and E. S. Polzik, 2010, "Quantum Noise Limited and Entanglement-Assisted Magnetometry," *Physical Review Letters* **104**, 133601. https://link.aps.org/doi/10.1103/PhysRevLett.104.133601

[61] I. M. Savukov, and M. V. Romalis, 2005, "Effects of spin-exchange collisions in a high-density alkali-metal vapor in low magnetic fields," *Phys. Rev. A* **71**, 023405. https://link.aps.org/doi/10.1103/PhysRevA.71.023405

[62] I. M. Savukov, 2017, in *Spin Exchange Relaxation Free (SERF) Magnetometers,* edited by Grosz, A., M. J. Haji-Sheikh, and S. C. Mukhopadhyay (Springer International Publishing, Cham), p. 451-491. https://doi.org/10.1007/978-3-319-34070-8_15

[63] W. E. Bell, and A. L. Bloom, 1961, "Optically Driven Spin Precession," *Phys. Rev. Lett.* **6**, 280-281. http://link.aps.org/doi/10.1103/PhysRevLett.6.280

[64] A. L. Bloom, 1962, "Principles of Operation of the Rubidium Vapor Magnetometer," *Applied Optics* **1**, 61. https://www.osapublishing.org/ao/abstract.cfm?uri=ao-1-1-61

[65] R. Jimenez-Martinez, W. C. Griffith, Y. Wang, S. Knappe, J. Kitching, K. Smith, and M. D. Prouty, 2010, "Sensitivity Comparison of Mx and Frequency-Modulated Bell–Bloom Cs Magnetometers in a Microfabricated Cell," *IEEE Transactions on Instrumentation and Measurement* **59**, 372-378. https://doi.org/10.1109/TIM.2009.2023829

[66] A. Predojević, Z. Zhai, J. M. Caballero, and M. W. Mitchell, 2008, "Rubidium resonant squeezed light from a diode-pumped optical-parametric oscillator," *Phys. Rev. A* **78**, 063820. https://link.aps.org/doi/10.1103/PhysRevA.78.063820

[67] R. Jiménez-Martínez, J. Kołodyński, C. Troullinou, V. G. Lucivero, J. Kong, and M. W. Mitchell, 2018, "Signal Tracking Beyond the Time Resolution of an Atomic Sensor by Kalman Filtering," *Phys. Rev. Lett.* **120**, 040503. https://link.aps.org/doi/10.1103/PhysRevLett.120.040503

[68] L. B. Madsen, and K. Mølmer, 2004, "Spin squeezing and precision probing with light and samples of atoms in the Gaussian description," *Phys. Rev. A* **70**, 052324. http://link.aps.org/doi/10.1103/PhysRevA.70.052324

[69] S. R. de Echaniz, M. W. Mitchell, M. Kubasik, M. Koschorreck, H. Crepaz, J. Eschner, and E. S. Polzik, 2005, "Conditions for spin squeezing in a cold 87Rb ensemble," *J. Opt. B* **7**, S548. http://iopscience.iop.org/article/10.1088/1464-4266/7/12/016/meta

[70] J. Kong, R. Jiménez-Martínez, C. Troullinou, V. G. Lucivero, G. Tóth, and M. W. Mitchell, 2020, "Measurement-induced, spatially-extended entanglement in a hot, strongly-interacting atomic system," *Nature Communications* **11**, 2415. https://doi.org/10.1038/s41467-020-15899-1

[71] I. Urizar-Lanz, P. Hyllus, I. L. Egusquiza, M. W. Mitchell, and G. Tóth, 2013, "Macroscopic singlet states for gradient magnetometry," *Phys. Rev. A* **88**, 013626. http://link.aps.org/doi/10.1103/PhysRevA.88.013626

[72] N. Behbood, F. Martin Ciurana, G. Colangelo, M. Napolitano, G. Tóth, R. J. Sewell, and M. W. Mitchell, 2014, "Generation of Macroscopic Singlet States in a Cold Atomic Ensemble," *Phys. Rev. Lett.* **113**, 093601. http://link.aps.org/doi/10.1103/PhysRevLett.113.093601

[73] G. Tóth, and M. W. Mitchell, 2010, "Generation of macroscopic singlet states in atomic ensembles," *New J. Phys.* **12**, 053007. http://stacks.iop.org/1367-2630/12/i=5/a=053007

[74] G. Tóth, C. Knapp, O. Gühne, and H. J. Briegel, 2007, "Optimal Spin Squeezing Inequalities Detect Bound Entanglement in Spin Models," *Physical Review Letters* **99**, 250405. https://link.aps.org/doi/10.1103/PhysRevLett.99.250405

[75] R. Jiménez-Martínez, J. Kolodynski, C. Troullinou, V. G. Lucivero, J. Kong, and M. W. Mitchell, 2017, "Signal tracking beyond the time resolution of an atomic sensor by Kalman filtering," *ArXiv e-prints*.

[76] J. Kitching, 2018, "Chip-scale atomic devices," *Applied Physics Reviews* **5**, 031302. https://doi.org/10.1063/1.5026238

[77] D. Sheng, S. Li, N. Dural, and M. V. Romalis, 2013, "Subfemtotesla Scalar Atomic Magnetometry Using Multipass Cells," *Physical Review Letters* **110**, 160802. https://link.aps.org/doi/10.1103/PhysRevLett.110.160802

[78] H. Crepaz, L. Y. Ley, and R. Dumke, 2015, "Cavity enhanced atomic magnetometry," *Scientific Reports* **5**, 15448. https://doi.org/10.1038/srep15448

[79] J. Kitching*, et al.*, 2016, "NIST on a Chip: Realizing SI units with microfabricated alkali vapour cells," *Journal of Physics: Conference Series* **723**, 012056. https://doi.org/10.1088%2F1742-6596%2F723%2F1%2F012056

[80] M. T. Hummon*, et al.*, 2018, "Photonic chip for laser stabilization to an atomic vapor with 1e-11 instability," *Optica* **5**, 443--449. http://www.osapublishing.org/optica/abstract.cfm?URI=optica-5-4-443

[81] S. J. Seltzer, *Developments in alkali-metal atomic magnetometry* 2008, Ph.D. thesis (Princeton University). http://proquest.umi.com/pqdweb?index=0&did=1642933481&SrchMode=2&sid=5&Fmt=2&VInst=PROD&VType=PQD&RQT=309&VName=PQD&TS=1234381973&clientId=17210

[82] T. Scholtes, S. Woetzel, R. Ijsselsteijn, V. Schultze, and H.-G. Meyer, 2014, "Intrinsic relaxation rates of polarized Cs vapor in miniaturized cells," *Applied Physics B* **117**, 211--218. https://doi.org/10.1007/s00340-014-5824-z

[83] M. E. Limes, E. L. Foley, T. W. Kornack, S. Caliga, S. McBride, A. Braun, W. Lee, V. G. Lucivero, and M. V. Romalis, 2020, "Portable magnetometry for detection of biomagnetism in ambient environments," *arXiv e-prints* arXiv:2001.03534. https://ui.adsabs.harvard.edu/abs/2020arXiv200103534L

[84] S. F. Huelga, C. Macchiavello, T. Pellizzari, A. K. Ekert, M. B. Plenio, and J. I. Cirac, 1997, "Improvement of Frequency Standards with Quantum Entanglement," *Phys. Rev. Lett.* **79**, 3865--3868. https://link.aps.org/doi/10.1103/PhysRevLett.79.3865

[85] V. G. Lucivero, W. Lee, M. E. Limes, E. L. Foley, T. W. Kornack, and M. V. Romalis, in 2019, (Optical Society of America), p. T3C.3. http://www.osapublishing.org/abstract.cfm?URI=QIM-2019-T3C.3

[86] S. Li, P. Vachaspati, D. Sheng, N. Dural, and M. V. Romalis, 2011, "Optical rotation in excess of 100 rad generated by Rb vapor in a multipass cell," *Phys. Rev. A* **84**, 061403. http://link.aps.org/doi/10.1103/PhysRevA.84.061403

[87] V. G. Lucivero, N. D. McDonough, N. Dural, and M. V. Romalis, 2017, "Correlation function of spin noise due to atomic diffusion," *Physical Review A* **96**, 062702. https://link.aps.org/doi/10.1103/PhysRevA.96.062702

[88] H. Y. Ling, 1994, "Theoretical investigation of transmission through a Faraday-active Fabry–Perot étalon," *Journal of the Optical Society of America A* **11**, 754-758. http://josaa.osa.org/abstract.cfm?URI=josaa-11-2-754

[89] K. G. Sycz, Wojciech; Zachorowski, Jerzy, 2010, "Resonant Faraday effect in a Fabry–Perot cavity," *Optica Applicata* **40**, 633-639. http://opticaapplicata.pwr.edu.pl/article.php?id=2010300633

[90] D. Hunger, T. Steinmetz, Y. Colombe, C. Deutsch, T. W. HŠnsch, and J. Reichel, 2010, "A fiber Fabry-Perot cavity with high finesse," *New Journal of Physics* **12**, 065038. https://doi.org/10.1088%2F1367-2630%2F12%2F6%2F065038

[91] M. Zhu, H. Wei, X. Wu, and Y. Li, 2015, "Fabry-Perot interferometer with picometer resolution referenced to an optical frequency comb," *Optics and Lasers in Engineering* **67**, 128--134. http://www.sciencedirect.com/science/article/pii/S0143816614002826